

*A DISSERTATION ON*

**“DEVELOPMENT OF IDF CURVES CONSIDERING  
THE IMPACT OF CLIMATE CHANGE FOR THE  
BARAK RIVER BASIN”**

*Submitted in Partial Fulfilment of the Requirements for the award of degree  
of*

**MASTER OF TECHNOLOGY  
CIVIL ENGINEERING  
*Specialization in*  
WATER RESOURCES ENGINEERING**

**Under  
ASSAM SCIENCE AND TECHNOLOGY UNIVERSITY  
*For the session 2022-2024***



*Submitted By*  
**MADHUSMITA HALOI**  
**Roll No. – 220620061007**  
**ASTU Registration No. - 000206222**

*Under the Guidance of*  
**DR. BHARATI MEDHI DAS**  
**ASSISTANT PROFESSOR**

**DEPARTMENT OF CIVIL ENGINEERING  
ASSAM ENGINEERING COLLEGE  
JALUKBARI, GUWAHATI-781013**



**DEPARTMENT OF CIVIL ENGINEERING  
ASSAM ENGINEERING COLLEGE  
JALUKBARI, GUWAHATI**

**DECLARATION**

The work contained in the report “**Development of IDF Curves Considering the Impact of Climate Change for the Barak River basin**” has been carried out by me under the supervision and guidance of **Dr. Bharati Medhi Das**, Assistant Professor, Department of Civil Engineering, Assam Engineering College, Guwahati.

Place: Guwahati

Dated:

**Madhusmita Haloi**

(220620061007)

M.Tech 4<sup>th</sup> Semester

Department of Civil Engineering

Assam Engineering College



**DEPARTMENT OF CIVIL ENGINEERING  
ASSAM ENGINEERING COLLEGE  
JALUKBARI, GUWAHATI**

**CERTIFICATE OF APPROVAL  
SESSION (2022-2024)**

**CERTIFICATE**

This is to certify that the project report entitled “**Development of IDF Curves Considering the Impact of Climate Change for the Barak River basin**” is a report submitted by Madhusmita Haloi, bearing roll no. 220620061007 under Assam Science and Technology University, Guwahati in partial fulfillment of the requirement for the award of degree of “**Master of Technology**” in Civil Engineering with Specialization in “**Water Resources Engineering**” is carried out by her under my supervision and guidance.

The work has been found quite satisfactory.

Place: Guwahati

Dated:

**Dr. Bharati Medhi Das**

Assistant Professor

Department of Civil Engineering

Assam Engineering College



**DEPARTMENT OF CIVIL ENGINEERING  
ASSAM ENGINEERING COLLEGE  
JALUKBARI, GUWAHATI**

**CERTIFICATE OF APPROVAL  
SESSION (2022-2024)**

**CERTIFICATE**

This is to certify that Madhusmita Haloi, student of 4<sup>th</sup> semester, bearing roll no. 220620061007, Master of Technology in Civil Engineering, Assam Engineering College has submitted the project report entitled **“Development of IDF Curves Considering the Impact of Climate Change for the Barak River basin”** in partial fulfillment of the requirement for the award of degree of **“Master of Engineering”** in civil engineering with Specialization in **“Water Resources Engineering”** under Assam Science and Technology University.

The Work has been found quite satisfactory.

Place: Guwahati

Dated:

**Dr. Jayanta Pathak**

Professor & Head

Department of Civil Engineering

Assam Engineering College

## ACKNOWLEDGEMENT

---

---

At the very outset, I am highly contented to express my sincere and heartfelt gratitude to my respected guide **Dr. Bharati Medhi Das**, Assistant Professor, Department of Civil Engineering, Assam Engineering College for providing me an opportunity to work under her supervision and guidance and also for her invaluable guidance, constructive suggestions and full cooperation throughout the course of this study and also in preparing and finalizing the report by her diligent scrutiny and correction of the manuscript.

I would also like to express my sincere and heartfelt gratitude to **Dr. Jayanta Pathak**, Professor and Head, Department of Civil Engineering, Assam Engineering College for his constant encouragement and for providing the necessary facilities to carry out the project work.

I would like to thank all the faculty members and staffs of the Department of Civil Engineering, Assam Engineering College for providing valuable help and support to carry out the works.

Place: Guwahati

Dated:

**Madhusmita Haloi**

(220620061007)

M.Tech 4<sup>th</sup> Semester

Department of Civil Engineering

Assam Engineering College

# ABSTRACT

---

---

An increase in greenhouse gases is thought to alter the hydrologic cycle, which in turn alters the frequency, length, and severity of precipitation events. Rainfall parameters, such as the Intensity-Duration-Frequency correlations, are often employed in water management infrastructure design, thus it is important to assess and update them for future climatic scenarios.

This research aimed to assess how the IDF curves in the Barak River Basin are likely to vary in response to future climate projections compared to the present.

The Statistical Downscaling Model (SDSM) was used to spatially downscale the HadCM3/GCM output predictor data under A2 and B2 emission scenarios, after collecting historically observed rainfall data. "After extracting maximum data series for 1, 2, 3, 6, 12, and 24-hour durations, the Intensity-Duration-Frequency Analysis was carried out. To select the best fitting distribution function, the data was fitted to the Gumbel, Log normal, and Log Pearson Type III distributions. The Log Pearson Type III was determined to be appropriate and was used to extrapolate rainfall intensity to generate Intensity-Duration-Frequency curves. Using the EasyFit programme, we ran the Kolmogorov-Smirnov, Anderson-Darling, and Chi-Squared tests to ensure that the probability distribution was well-fitted. The research region's average Intensity-Duration-Frequency curve was developed by calculating the Thiessen polygon area for each station using ArcGIS.

At last, we have a link between average intensity, duration, and frequency of rainfall that we can use to predict how heavy the rain will be in the future. The present climate's spatial fluctuation in rainfall intensity may be seen on isopluvial maps. Next, for the future time lines (2011–2030 and 2031–2050), we assessed the relative differences in rainfall intensity between the present and future climatic scenarios. For both future epochs, this study's findings point to less heavy rainfall.

# CONTENTS

---

---

<b>PARTICULARS</b>	<b>PAGE NOS.</b>
<b>DECLARATION</b>	<b>i</b>
<b>CERTIFICATE OF APPROVAL</b>	<b>ii</b>
<b>CERTIFICATE OF APPROVAL</b>	<b>iii</b>
<b>ACKNOWLEDGEMENT</b>	<b>iv</b>
<b>ABSTRACT</b>	<b>v</b>
<b>CONTENTS</b>	<b>vi</b>
<b>LIST OF FIGURES</b>	<b>ix</b>
<b>LIST OF TABLES</b>	<b>x</b>
<b>ABBREVIATIONS</b>	<b>xii</b>
<b>NOTATIONS</b>	<b>xiii</b>
<b>CHAPTER 1: INTRODUCTION</b>	<b>1-10</b>
<b>1.1 INTRODUCTION</b>	<b>1</b>
<b>1.2 CLIMATE CHANGE</b>	<b>1</b>
<b>1.3 GLOBAL CIRCULATION MODELS (GCMS)</b>	<b>1</b>
<b>1.4 DOWNSCALING MODELS</b>	<b>2</b>
1.4.1 STATISTICAL DOWNSCALING	2
1.4.2 DYNAMIC DOWNSCALING	3
<b>1.5 CLIMATE CHANGE SCENARIOS</b>	<b>3</b>
1.5.1 EMISSION SCENARIOS	3
<b>1.6 OVERVIEW OF STATISTICAL DOWNSCALING MODEL SOFTWARE (SDSM 4.2.9)</b>	<b>4</b>
<b>1.7 RAINFALL INTENSITY-DURATION-FREQUENCY CURVES</b>	<b>5</b>
1.7.1 LOGNORMAL DISTRIBUTION	6
1.7.2 GUMBEL DISTRIBUTION	6
1.7.3 LOG PEARSON TYPE III DISTRIBUTION	7
1.7.4 PROBABILITY PLOTTING POSITION	8
<b>1.8 DERIVATION OF INTENSITY-DURATION-FREQUENCY EQUATION</b>	<b>8</b>

<b>1.9 PROBLEM DEFINITION IN THE STUDY AREA</b>	9
<b>1.10 OBJECTIVES</b>	9
<b>CHAPTER 2: LITERATURE REVIEW</b>	<b>11-15</b>
<b>2.1 INTRODUCTION</b>	11
<b>2.2 INTENSITY-DURATION-FREQUENCY CURVES</b>	11
<b>2.3 CLIMATE CHANGE</b>	11
<b>2.4 PREVIOUS RESEARCH</b>	12
<b>CHAPTER 3: STUDY AREA AND DATABASE</b>	<b>16-20</b>
<b>3.1 DESCRIPTION</b>	16
3.1.1 SALIENT FEATURES OF BARAK AND OTHER BASINS	18
<b>3.2 DATABASE</b>	19
<b>CHAPTER 4: METHODOLOGY</b>	<b>21-28</b>
<b>4.1 INTRODUCTION</b>	21
<b>4.2 DATA PRE-PROCESSING</b>	21
4.2.1 DAILY RAINFALL DISAGGREGATION METHOD	21
4.2.2 CONSISTENCY ANALYSIS	22
<b>4.3 BUILDING CLIMATE CHANGE SCENARIOS</b>	22
4.3.1 GLOBAL CIRCULATION MODEL (CGM)	22
4.3.2 CLIMATE CHANGE SCENARIOS	22
4.3.3 STATISTICAL DOWNSCALING MODEL (SDSM) PROCEDURES	22
<b>4.4 INTENSITY-DURATION-FREQUENCY ANALYSIS</b>	23
4.4.1 FITTING THE PROBABILITY DISTRIBUTION	23
4.4.2 TESTING THE GOODNESS OF FIT DATA	24
4.4.3 COMPUTATION OF EXTREME EVENTS ( $X_T$ )	25
4.4.4 CALCULATING INTENSITY OF RAINFALL (I)	26
<b>4.5 DERIVATION OF IDF EQUATION</b>	26
<b>4.6 DEVELOPING ISOPLUVIAL MAPS</b>	27

4.7 COMPARISON OF INTENSITY DURATION FREQUENCY RESULTS	28
<b>CHAPTER 5: RESULTS AND DISCUSSIONS</b>	<b>29-46</b>
5.1 INTRODUCTION	29
5.2 CONSISTENCY ANALYSIS OF THE RAINFALL DATA SERIES	29
5.3 CLIMATE CHANGE SCENARIOS OF RAINFALL	29
5.3.1 SELECTED ATMOSPHERIC PREDICTOR VARIABLES	29
5.3.2 CALIBRATION AND VALIDATION OF THE MODEL	30
5.4 GENERATION OF IDF CURVES	31
5.4.1 DISAGGREGATION OF DAILY RAINFALL	32
5.4.2 SELECTION OF BEST FITTING PROBABILITY DISTRIBUTION FUNCTION	33
5.4.3 GOODNESS OF FIT OF DATA	35
5.4.4 COMPUTED EXTREME RAINFALL QUANTILES ( $X_T$ )	36
5.4.5 COMPUTED RAINFALL INTENSITIES (I)	38
5.4.6 MATHEMATICAL EXPRESSION OF IDF CURVES	43
5.5 GENERATION OF ISOPLUVIAL MAPS	44
5.6 COMPARISON OF IDF RESULTS	46
<b>CHAPTER 6: CONCLUSION</b>	<b>48-49</b>
6.1 CONCLUSION	48
6.2 SCOPE OF FURTHER STUDY	49
<b>REFERENCES</b>	<b>50-51</b>

# LIST OF FIGURES

---

---

FIGURE NO.	CAPTION	PAGE NOS.
3.1	Barak and other basins	14
3.2	Location map of study area	15
3.3	Location of rain gauge stations used in the study area	16
5.1	Thiessen Polygon map of the study area	20
5.2	IDF curve for current climate (1979-2013)	27
5.3	IDF curve for A2 scenario (2011-2030)	28
5.4	IDF curve for B2 scenario (2011-2030)	28
5.5	IDF curve for A2 scenario (2031-2050)	29
5.6	IDF curve for B2 scenario (2031-2050)	29
5.7	Isopluvial map for 30 minutes of 100 years return period for current climate	46
5.8	Isopluvial map for 1 hour of 100 years return period for current climate	47
5.9	Isopluvial map for 2 hour of 100 years return period for current climate	47
5.10	Isopluvial map for 3 hour of 100 years return period for current climate	48
5.11	Isopluvial map for 6 hour of 100 years return period for current climate	48
5.12	Isopluvial map for 12 hour of 100 years return period for current climate	49
5.13	Isopluvial map for 24 hour of 100 years return period for current climate	49

# LIST OF TABLES

TABLE NO.	CAPTION	PAGE NOS.
3.1	Location of the Rain Gauge Stations	20
4.1	Description of goodness-of-fit tests	21
5.1	Selected predictor variables	25
5.2	Performance of model during calibration period	25
5.3	Performance of model during validation period	25
5.4	R-squared values for AMS	28
5.5	Goodness of fit for Log Pearson Type III distribution for station 242928	30
5.6	Computed rainfall quantiles $X_T$ (mm) using historic data of current climate for different return periods and durations	31
5.7	Computed rainfall quantiles $X_T$ (mm) using A2 scenario data of 2011-2030 for different return periods and durations	31
5.8	Computed rainfall quantiles $X_T$ (mm) using B2 scenario data of 2011-2030 for different return periods and durations	31
5.9	Computed rainfall quantiles $X_T$ (mm) using A2 scenario data of 2031-2050 for different return periods and durations	32
5.10	Computed rainfall quantiles $X_T$ (mm) using B2 scenario data of 2031-2050 for different return periods and durations	32
5.11	Computed intensity of rainfall, $I$ (mm/hr) for current climate (1979-2013)	32
5.12	Computed intensity of rainfall, $I$ (mm/hr) for A2 scenario (2011-2030)	33
5.13	Computed intensity of rainfall, $I$ (mm/hr) for B2 scenario (2011-2030)	33
5.14	Computed intensity of rainfall, $I$ (mm/hr) for A2 scenario (2031-2050)	33
5.15	Computed intensity of rainfall, $I$ (mm/hr) for B2 scenario (2031-2050)	34
5.16	IDF relationships under different climate scenarios	37
5.17	Relative difference (RD) in intensity of rainfall from the current	40

	climate for A2 scenario (2011-2030) for different return periods	
5.18	Relative difference (RD) in intensity of rainfall from the current climate for B2 scenario (2011-2030) for different return periods	40
5.19	Relative difference (RD) in intensity of rainfall from the current climate for A2 scenario (2031-2050) for different return periods	40
5.20	Relative difference (RD) in intensity of rainfall from the current climate for B2 scenario (2031-2050) for different return periods	41

# ABBREVIATIONS

---

---

<b>ABBREVIATION</b>	<b>MEANING</b>
AMS	Annual Maximum Series
A-D	Anderson-Darling
CCISC	Canadian Climate Impacts and Scenarios
GCM	Global Circulation Model
GHG	Greenhouse gases
GIS	Geographic Information System
GOF	Goodness of fit
HadCM3	Hadley Centre Coupled Model, version 3
HadCM3A2	Hadley Centre Coupled Model, version 3, for the A2 emission scenario
HadCM3B2	Hadley Centre Coupled Model, version 3, for the B2 emission scenario
IDF	Intensity-Duration-Frequency
IDW	Inverse Distance Weighing
IPCC	Intergovernmental Panel on Climate Change
PDF	Probability Density Function
RD	Relative Difference
IMD	Indian Meteorological Department
K-S	Kolmogorov-Smirnov
LN	Lognormal
LPTIII	Log Pearson Type III
NCEP	National Centre for Environmental Prediction
RCM	Regional Circulation Model
SDSM	Statistical Downscaling Model
SRES	Special Report on Emission Scenarios

# NOMENCLATURE

---

---

<b>SYMBOL</b>	<b>DESCRIPTION</b>
C	Location
$C_s$	Skewness Co-efficient
$D_i$	Duration
e	Shape
I	Rainfall Intensity
$K_T$	Frequency Factor
m	Size
P	Probability of Exceedance
R	Rainfall
$R^2$	Coefficient of Determination
$T_d$	Period Measured
$T_r$	Return Period
$X_T$	Extreme Event
$Y_T$	Reduced Variate
Z	Standard Normal Variable
$\sigma$	Standard Deviation

# CHAPTER 1

## INTRODUCTION

---

---

### 1.1 INTRODUCTION

As the primary cause of climate change and global warming, human activities have increased the atmospheric concentration of carbon dioxide, which is expected to alter the hydrologic cycle by changing the frequency, duration, and intensity of precipitation events. Because of these shifts in temperature and precipitation, the hydrological cycle on Earth is no longer operating at its natural balance.

### 1.2 CLIMATE CHANGE

There are a number of industries that water resource managers work in that might be impacted by climate change. Rising sea levels and their consequences, as well as shifts in the patterns of precipitation and temperature, are the primary forces at work. Identifying and preparing for the potential effects of climate change is one way to lessen susceptibility. Since these characteristics are usually used to develop water management systems, it is necessary to review and update rainfall characteristics (i.e., Intensity-Duration-Frequency curves) for future climatic scenarios. In light of the fact that our planet's climate is rapidly changing, it is imperative that local governments investigate and implement effective strategies for dealing with and adapting to these new realities.

### 1.3 GLOBAL CIRCULATION MODELS (GCMs)

The integration of greenhouse gases (GHGs) and aerosols in Global Circulation Models (GCMs) allows for the simulation of both the current and future climates. Using the 'downscaling approaches,' one may get the daily precipitation corresponding to regional or local future climatic scenarios from GCM outputs, even if GCM spatial resolution is still very coarse. When it comes to predicting weather conditions like temperature, precipitation, wind speed, pressure, humidity, and solar radiation, these models are your

best bets right now. While it is well-established that GCM accuracy declines with increasing spatial and temporal resolution (usually between 250 and 600 km), the need for IDF analysis rises with decreasing resolution. Although some models provide parameters, others do not include information on the terrain, land use, or water distribution. Studies have shown that these models don't do a good job of simulating the monthly rainfall quantities that we see today or predicting the very variable daily rainfall. (Peck et al., 2013).

## **1.4 DOWNSCALING MODELS**

Compared to regional or global climate models, the spatial resolution needed for climate change impact assessments is much higher (Wilby and Dawson, 2007). While regional climate models (RCMs) may be as detailed as tens of kilometres, global circulation models (GCMs) can cover hundreds of km. The equivalence of point observations is necessary for many impact procedures, however. Consequently, it has to be shrunk to a more manageable size for the town. To get a better resolution from the GCM findings, you may use either statistical or dynamical downscaling.

### **1.4.1 STATISTICAL DOWNSCALING**

Robert Wilby and Christian Dawson developed the SDSM, or Statistical Downscaling Model. Multiple linear regression and stochastic downscaling are also incorporated. By comparing atmospheric variables measured at the right scale with those measured at the bigger (GCM) scale, statistical downscaling hopes to develop statistical correlations. By comparing the GCM output with this statistical connection, we may model local climate conditions, assuming that it will hold true for the future. Despite being computationally inexpensive, generating many representations rapidly, and applicable at any scale as far as observations are concerned, the results may not be physically coherent because the method assumes the statistical relationships for the current climate will remain valid in future changing conditions. Changes in land cover are an example of a small-scale process with substantial time-scale linkages that it ignores.

### **1.4.2 DYNAMIC DOWNSCALING**

"Dynamic downscaling" is a way to model climate change by incorporating a wide range of meteorological variables and fluxes into an environmental model, including

but not limited to wind speed and direction, soil moisture, runoff, temperature, and relative humidity. To predict the impact of global patterns on local weather, dynamic downscaling uses numerical meteorological models. In order to downscale the GCM findings to a finer scale, it makes use of Regional Climate Models (RCMs) with better resolution. The RCM takes as input either GCM or reanalysis data and, similar to the GCMs, generates geographically and temporally coherent variables, but with a finer granularity. The computing cost, skill, and storage resources needed for this technology are significant drawbacks. It takes a long time to complete the simulations.

## **1.5 CLIMATE CHANGE SCENARIOS**

The Hadley Centre for Climate Prediction and Research in England (HadCM3) and the Canadian Centre for Climate Modelling and Analysis (CGCM2) are the two most widely used general circulation meteorological (GCM) models. In order to facilitate impact research, the results of these models are made available online. The four primary components of more recent GCMs—air, water, land, and ice—form a connected model. Assumptions on demographic shifts, economic growth, technological development, and the effects of political and social globalisation form the basis of each scenario. The details of the six emission scenarios proposed by the Special Report on Emission Scenarios (SRES)—A1F1, A1T, A1B, A2, B1, and B2—are covered in Section 1.4.1. To put it simply, scenarios are neither forecast or predictions of the future. Rather, they provide a picture of potential futures that vary according to the limits or conditions that make them feasible. If the present climate is different from a climate scenario, then we have a climate change scenario. (IPCC, 2007a).

### **1.5.1 EMISSIONS SCENARIOS**

Future emissions of aerosols and greenhouse gases into the atmosphere will be greatly affected by factors such as population and economic development, energy consumption, and other such metrics. Based on whether the scenarios were motivated by environmental concerns rather than economic ones, the emphasis on global or regional growth, and the number of families into which they fall, it is possible to categorise them. The commonly known outline is given here for reference (Tesfaye, 2014).

**A1:** Globalisation is driving rapid economic growth; the world's population reaches its maximum around mid-century and then begins to decline; wealth as a whole increase; and regional income gaps shrink and convergence takes place. Various branches of this family postulate various energy sources to power this exponential expansion: A1B, which assumes a balance between all sources, A1T, which postulates non-fossil fuels, and A1FI, which postulates fossil fuels exclusively. Being balanced means not putting all of your eggs in one basket of energy sources. This is based on the premise that all energy supply and end use technologies will continue to increase at the same pace.

**B1:** Similar to A1 in terms of population growth, but development follows a far greener course via international collaboration and regulation. New technologies are developed that are both clean and efficient. Achieving sustainability on all fronts—economic, social, and environmental—requires a global approach.

**A2:** A market-led, diverse environment where population expansion is outpacing economic development since fertility rates aren't converging as quickly. The key idea is being true to one's roots and being self-sufficient. Because economic growth is concentrated in some regions, there is a wide range of income growth and technical development from one area to another.

**B2:** Development follows regionally directed routes that are ecologically, economically, and socially sustainable, and the population grows at a slower pace than A2 but faster than A1 and B1. B1 and B2 are on opposite ends of the spectrum when it comes to the impact on global warming. The A1F1 scenario, which relies heavily on fossil fuels, is the most forcing, followed by A2.

## **1.6 OVERVIEW OF STATISTICAL DOWNSCALING MODEL SOFTWARE (SDSM 4.2.9)**

Statistical Downscaling Model (SDSM) is a decision-support tool for assessing the local consequences of climate change through the statistical downscaling technique. This technique, as described by Wilby and Dawson (2007), incorporates features of multiple regression and stochastic weather generator to generate new characteristics from pre-existing data.

Climate change scenarios may be developed utilising grid resolution of GCM data at daily time-scales using the statistical downscaling model (SDSM). After establishing the statistical association between global climate parameters (predictors) and local variables (predictands), the next step is to simulate local climate data and create future climate change scenarios. There are many different kinds of statistical downscaling approaches, but they always fall into one of three categories: weather typing schemes, stochastic weather generators, and regression (transfer function) methods.

## 1.7 RAINFALL INTENSITY-DURATION-FREQUENCY CURVES

Accurate estimates of rainfall intensity are necessary for hydrologic studies, as well as for planning and design purposes. It is common practice to utilise intensity-duration-frequency (IDF) curves to assess rainfall in planning pertaining to water resources. An effective tool for predicting the excessive rainfall in the target area, IDF curves show the typical rainfall intensity over all return periods and durations. If you want to build channels or other waterways, you may utilise IDF curves to figure out the catchment's peak runoff using the rational technique. Due to their use in the rational formula, the IDF curves are employed to predict peak run-off rates. For the purpose of designing bridges and spillways, the curves are also fed into rainfall-runoff models that generate massive floods. Similarly, accurate forecasts of rainfall intensities form the basis of soil erosion control methods and irrigation management processes.

The IDF curves are often produced by doing annual maximum studies of historical precipitation data, presuming no change in the climate. The regional IDF distribution was ascertained using a frequency analysis of rainfall intensity during various time intervals and return periods. We employed three distinct probability distributions to fit the rainfall measurements: the Gumbel, the Lognormal, and the Log Pearson Type III.

In equation (1.1), we can see the connection between the return period ( $T_r$ ) and the chance of exceedance ( $P$ ) of a rainfall event:

$$T_r = \frac{1}{P} \tag{1.1}$$

If the extreme event ( $X_T$ ) for any particular year is equal to or more than a certain value, then the probability of exceedance ( $P$ ) is high. Alternatively, the time it takes for an event to be met or surpassed twice is known as the return period ( $T_r$ ). The moment, L-

Moment, or likelihood approaches are used to determine  $X_T$  according to the postulated probability distribution (Hosking and Wallis, 1993). On the other hand, it may be calculated for the probability distribution functions in (1.2) using frequency factors (Das et al., 2016):

$$X_T = \overline{X_T} + K_T \sigma \quad (1.2)$$

where  $X_T$ . and  $\sigma$  are the variate's mean and standard deviation, and  $K_T$  is the frequency factor that depends on the distribution parameter and return time.

### 1.7.1 LOGNORMAL DISTRIBUTION

Similar to the normal distribution, the lognormal distribution uses the logarithm of the dependent variable ( $y = \log(x)$ ) instead of the actual value of the variable ( $x$ ). The Lognormal distribution is defined by its strong positive skew and its left-hand boundary of zero. Many frequency distributions derived from hydrologic data analysis have both of these features. Here is the normal distribution's probability density function (PDF) after a logarithmic transformation:

$$f(x) = \frac{1}{x\sigma_y\sqrt{2\pi}} \exp\left(-\frac{1}{2\sigma_y^2} [y - \bar{y}]^2\right) \quad x > 0 \quad (1.3)$$

where the sample's reduced variate's mean and standard deviation are represented by the variables  $y = \log(x)$ .  $\bar{y}$ , and  $\sigma_y$ . The log-normal distribution has two advantages over the normal distribution: a constraint known as  $x > 0$  and a general trend towards less positive skewness.

### 1.7.2 GUMBEL DISTRIBUTION

The probability of an event with a value equal to or greater than  $x_o$ , as stated in Reddi's (2002) theory of maximum events, is:

$$P(x \geq x_o) = 1 - e^{-e^{-y}} \quad (1.4)$$

where,  $y = \alpha(x - \beta)$  is called the *reduced variable*. According to Reddi (2002), the following equations connect the parameters of the variate  $x$ ,  $\bar{x}$ , and  $\sigma$  to its mean and standard deviation:

$$\alpha = \frac{1.28255}{\sigma} \quad (1.5)$$

$$\beta = \bar{x} - 0.45005\sigma \quad (1.6)$$

the parameters of the distribution are denoted as  $\alpha$  and  $\beta$ .

### 1.7.3 LOG PEARSON TYPE III DISTRIBUTION

The log-Pearson distribution is a type III distribution that is derived from the gamma distribution by its logarithmic transformation. When  $x$ 's logarithm follows a Pearson Type III distribution, we say that the distribution is logarithmic. An intriguing feature is that when  $\log x$  is symmetric around its mean, the Log Pearson distribution simplifies to a normal distribution. When it comes to assessing rainfall intensities and the frequency of yearly maximum floods, this distribution is often considered the gold standard for many nations. The PDF is given by (Asgele, 2014):

$$f(x) = \frac{\lambda^\beta (y - \varepsilon)^{\beta-1} e^{-\lambda(y-\varepsilon)}}{x\Gamma(\beta)} \quad \log x \geq \varepsilon \quad (1.7)$$

where  $y = \log x$  and  $\lambda$ ,  $\beta$ , and  $\varepsilon$  are the distribution's scale, shape, and placement parameters.,  $\Gamma(\beta) = (\beta - 1)!$ ,  $\lambda = \frac{S_y}{\sqrt{\beta}}$ ,  $\beta = \left( \frac{2}{C_s(y)} \right)^2$ , and  $\varepsilon = \bar{y} - S_y \sqrt{\beta}$  assuming the skewness  $C_s(y)$  is positive. The skew coefficient ( $C_s(y)$ ) is determined using the expression:

$$C_s(y) = \frac{n \sum_{i=1}^n (y_i - \bar{y})^3}{(n-1)(n-2)(n-3)} \quad (1.8)$$

$$\mu_y = \varepsilon + \lambda\beta, \quad \delta_y = \lambda\sqrt{\beta}, \quad \text{and} \quad C_s(y) = 2\sqrt{\beta} \quad (1.9)$$

The population's sample estimates, where  $n$  is the number of observations, are computed

using the parameters  $\lambda$ ,  $\beta$ , and  $\varepsilon$  as the mean  $\mu_y$ , standard deviation  $\delta_y$ , and coefficient of skew  $C_s$ .

#### 1.7.4 PROBABILITY PLOTTING POSITION

By computing their Plotting Positions for a particular record length, we may find the probability distribution of hydrologic data. One of the primary goals of probability frequency analysis is to determine the correlation between storm intensity and occurrence frequency. There is no consensus on the best way to calculate plotting position probability, despite the fact that several alternative formulae have been suggested. Assigning a rank number ( $m$ ) to each occurrence and sorting them in decreasing order of magnitude is the simplest approach. The Weibull formula, as stated by Chow et al. (1988), is the most often utilised formula in this research.

$$P(x) = \left( \frac{m}{n+1} \right) \rightarrow T_r = \left( \frac{n+1}{m} \right) \quad (1.10)$$

in where  $m$  is the event's rank number,  $n$  is the entire sample size of a particular record, and  $T_r$  is the recurrence interval, and  $P(x)$  is the probability of exceedance.

### 1.8 DERIVATION OF IDF EQUATION

Maximum rainfall intensity is the dependent variable in the IDF formulas, whereas rainfall duration and frequency are the independent variables that are crucial to the relationship. Chow et al. (1988) states that the variables previously discussed are related by a number of functions that are frequently employed in hydrological application literature. Here is the general form of an empirical equation:

$$I = \frac{CT_r^m}{T_d^e} \quad (1.11)$$

where  $I$  is the average intensity of rainfall for the given time period The return period is denoted as  $T_d$ ,  $T_r$ . The location, shape, and size of the region are crucial in determining the empirical parameters  $C$ ,  $e$ , and  $m$ , which are in turn determined by the area's properties and precipitation data through logarithmic relationships.

## **1.9 PROBLEM DEFINITION IN THE STUDY AREA**

The average annual surface temperature of the Earth has increased by about 0.3 to 0.6 degrees Celsius since the late 1800s, according to current scientific study. Coulabaly and Xhi (2005) state that the IPCC projects an additional 1 to 3.5 degrees Celsius increase in this temperature over the next century. The hydrologic cycle is expected to undergo alterations, which could lead to changes in the frequency and intensity of extreme weather events. We used Sen's slope model to estimate the amount of change in the Barak River Basin and the Mann-Kendall test to uncover patterns in the basin. From 1901 to 2010, the Barak basin experienced a significant decrease in monsoon and post-monsoon rainfall, according to the results. The annual and monsoon rainfall in the basin has decreased significantly during the past 30 years. The likelihood of severe floods or brief droughts is higher when the amplitudes of recent rainfall changes are bigger (Deka et al., 2012). The amount of the design discharge will fluctuate as a consequence of climate change, which might have negative impacts on current drainage infrastructure if it causes precipitation intensities to rise or fall. Whether or not new drainage design standards should be established to accommodate the effects of the anticipated climate change is an important question that these raises.

Although the Barak River Basin may produce a lot of electricity, it is currently underdeveloped and not making the most of its water resources (Bora and Choudhury, 2015). A few issues that affect the basin include flooding, clogged drainage systems, and bank erosion. Excessive rainfall in the area, the main river's backing up on its tributaries, and the channels' limited carrying capacity as a consequence of river bed aggravation are the major causes of flooding. Many depressions continue to be flooded long after the monsoon has passed because of inadequate drainage. Consequently, in order to plan and manage projects pertaining to water resources, it is necessary to conduct hydrological analyses in both the current and future climatic scenarios.

## **1.10 OBJECTIVES**

The current study's overarching goal is to provide some insight into how severe rainfall occurrences may evolve in the future and to propose techniques for measuring precipitation. The result is displayed using likelihood-based Intensity-Duration-Frequency (IDF) curves that are appropriate for the approaching weather conditions.

This study attempted to examine the intensity, duration, and frequency of rainfall under shifting climate scenarios by assessing the change in IDF curves for two climate scenarios (A2 and B2). This study set out to predict how the Barak River Basin will react to future climate change so that engineers could better plan and build hydraulic infrastructure to deal with the predicted effects. Specifically, the research aimed to achieve:

- To develop IDF curve under current climatic condition
- To create IDF curves for two potential future climate scenarios (A2 and B2) and then compare them to the existing IDF curve.

# CHAPTER 2

## LITERATURE REVIEW

---

---

### 2.1 INTRODUCTION

When it comes to recent climatic writings, climate change is among the most talked-about issues (assuming we include global warming in our definition). Among climate change-related publications, the most well-known one is the IPCC report. A change in the climate that is either directly or indirectly induced by human activities altering the composition of the global atmosphere is referred to as climate change. This includes both natural climatic fluctuation and changes observed across comparable time periods.

Climate change has the potential to affect many different things, including the accessibility of water resources. Rising sea levels and their consequences, as well as shifts in the patterns of precipitation and temperature, are the primary forces at work.

In urban drainage planning and floodplain management, one of the most used strategies is the rainfall intensity-duration-frequency relationship. Knowing both the intended use of the building and the specifics of its surrounding environment are crucial to the design process of any infrastructure project. Storm water management uses the length of time that heavy rains last as a measure to choose the right size of infrastructure parts. The IDF curves that come from statistical analyses of exceptional occurrences are a common way to represent this data.

An overview of the previous researches on this topic, that are available in literature, is presented in this chapter.

## 2.2 PREVIOUS RESEARCH

- **Coulibaly and Shi (2005)** utilised CGCM2 B2 and the statistical downscaling method SDSM to create IDF curves for the Grand River and Kenora Rainy River basins in Ontario. Data from all locations showed that the intensity of rainfall during 24-hour and sub-daily periods rose by 24-35% in the 2050s and 2080s, but fell in the 2020s. An upward trend is evident for the maximum annual precipitation at three of the four stations located in the Grand River Region, all four sites in the Kenora Region, and the Rainy River Region.
  
- **Sarkar et al. (2009)** set out to develop regional IDF curves for the Indian Himalayan region of Tehri-Garhwal. The IDF curves were constructed with four stations' worth of data, and the L-moments method was used to analyse each station individually. The LPT III distribution worked well with the rainfall data. The most extreme envelope curves were drawn out to depict the potential intensity of the rainfall. We used the Thiessen polygon method to build an average IDF curve, but we lost the geographical diversity of the data. As a result, the Bhagirathi-Bhillangana catchment area's spatial variability was shown on isopluvial maps, and IDF connections were then established. The study concluded that if rainfall intensity values are required as an input to a model for entire catchment, the empirical formula  $I = 21.76 \frac{T^{0.281}}{(t-0.2)^{0.55}}$  could be used. For site specific rainfall values, isopluvial maps could be used.
  
- **Mirhosseini et al. (2012)** compared IDF curves created for Alabama under present and future climatic scenarios. This research used six projections that were dynamically downscaled. The findings imply that the return period determines whether the intensity of subsequent rainfall decreases or increases. Because climate models' predictions of future rainfall intensities are fraught with high uncertainty over long time periods, it is difficult to draw any firm conclusions about the expected consequences. The different results could be due to a number of factors, such as the fact that different GCMs and RCMs use different physical parameterizations (particularly for radio-active and precipitation-forming processes) and have different starting and boundary conditions for their climate projections. Regardless, all of the

models appear to agree that the pattern of precipitation is shifting towards less intense rainfalls for shorter durations (less than 4 hours).

- For IDF analysis, the most common probability distributions used are the Gumbel and Log Pearson Type 3 distributions. **Ewea et al. (2016)** conducted IDF analysis using the Gumbel distribution approach for high-value occurrences such as unpredictable precipitation in dry locations. Closed IDF values were obtained using Gumbel and LPT III in the Riyadh area (Al-Hassoun 2011) and in some KSA localities (Al-Shaikh 1985). A few studies have shown that Gumbel's estimates of rainfall intensity are a little larger than the LPT III distribution (Dar and Maqbool, 2016). Researchers like Subyani and Al-Amri found no significant difference between Gumbel and LPT III in their investigations carried out in the city of Al-Madinah in western Saudi Arabia (2015). New and intriguing studies are cropping up on the topic of creating IDF values using techniques other than the distribution fit.
- To determine the IDF linkages for homogeneous areas in Botswana, which quantify the intensity, duration, and frequency of rainfall, **Alemaw and Chaoka (2016)** conducted a regional analysis of design storms. The K-Means Clustering technique was used to build three homogenous zones based on topography and rainfall parameters.
- To create the IDF curves using an empirical equation (**Kothyari and Garde**), **Zope et al. (2016)** initially proposed using a probability distribution for yearly maximum rainfall. The revised formula enables the creation of IDF curves that function admirably in a range of hydrologic scenarios, such as the exceptionally severe downpour that hit Mumbai on July 26, 2005. Conversely, the entire city may make use of the IDF link that was developed for the Santacruz rain gauge station. Its central location and ability to measure greater rainfall intensities make it a good candidate for future flood prevention.
- Using data gathered from 26 rainfall gauging stations, **Wagesho and Claire (2016)** aimed to construct a rainfall IDF connection for the whole Rwanda. Utilising the moment ratio and L-moment ratio diagrams, we were able to align the frequency

distribution with the observed 24-hour annual maximum rainfall data and identify homogeneous zones. Every station was given one of five standard locations. To estimate the quantiles for all stations in a specific area, we have employed the best-fit regional distribution for various return periods using Generalised Logistic, Gamma, Pearson Type II, and Generalised Extreme Value. The quantile for a certain area is then determined by averaging the quantiles for all of the stations in that area. There was no clearly established association with regard to a station local, but the IDF parameters show commonality during the return time.

- Using a variety of return intervals and durations, **Carlier and Khattabi (2016)** investigated how rising temperatures affected the intensity of rainfall in Toronto. It was noted that there was a significant rise in temperature after 1980. We have calculated and compared the IDF curves before and after 1980 using the Gumbel Extreme Value distribution. The impact of global warming on the IDF curves was not immediately obvious, even though rainfall intensity declined after 1980, especially for shorter durations. This finding disproves the existence of a universal rule and demonstrates instead that the impact of climate change on precipitation differs according to longitude and latitude.
- **Das et al. (2016)** constructed the IDF curve for Guwahati city by utilising Gumbel's Extreme Value distribution. For this study, we collected rainfall data with shorter time intervals. IDF empirical formula  $i = a * (t_d)^{-c}$  was used in the study for estimating the maximum rainfall intensities for different duration and return periods. The IDF parameters a and c can be used to find out how much rain fell over a specific time frame. The calculated data reveals that rainfall intensity declines with increasing length, but for a given duration, it tends to rise as return period grows.
- Maximum yearly rainfall for the 2020s, 2050s, and 2080s was calculated by **Kouk et al. (2016)** using the following algorithms: Cuckoo search optimisation, neural network (NN) with scale conjugate gradient, and Statistical Downscaling Model (SDSM). According to the findings, future IDF curves will be somewhat larger than their predecessors.
- In their analysis, **Akbari et al. (2016)** used the HadCM3 and CGCM3 GCMs along with three statistical downscaling methods: the Statistical Down Scaling Model

(SDSM), the Long Ashton Research Station Weather Generator (LARS-WG), and the Change Factor (CF). The study was conducted under the A2 emission scenario. For the base era (1971–2000) and subsequent periods, IDF curves were created. Rainfall intensities with short durations (1 hour and 3 hours) decreased while those with long durations (6, 9, and 12 hours) increased when comparing the base and future periods.

- In order to take into consideration all potential Representative Concentration Pathways (RCP) scenarios, **Singh et al. (2016)** aimed to update the IDF curves for an Indian town using five GCMs. The equidistant quantile method was used to probe the relationships between historical, contemporary, and future GCM data, as well as historical, contemporary, and future GCM data and observed sub-daily data. The anticipated sub-daily intensities were derived from this connection. All of the RCP scenarios showed an increase in rainfall intensity when analysing the IDF curves. A further finding is that when RCP scenarios are more intense, the intensities of all return periods get stronger.

# CHAPTER 3

## STUDY AREA AND DATABASE

---

---

### 3.1 DESCRIPTION

Rising in the hill region of Manipur State, the Barak River—the largest and most significant of the hill country rivers—is a key river in southern Assam, India. With its headwaters in the Japvo mountain range of the Manipur highlands, the Barak River flows south through Assam before emptying into the Bay of Bengal as the Meghna, a tributary of the Brahmaputra. The Naga and Lushai hills form its eastern boundary, the Barail range its northern one, and the Bangladeshi plains its southern and western ones. Assam, Manipur, Mizoram, Nagaland, and Tripura are all parts of the Barak Basin. The Surma-Meghna River System, which includes the rivers Kushiya and Surma, originates in Bangladesh after leaving Assam. In northeastern Bangladesh, the Barak River is the most important river by volume. The Jiri, Dhaleshwari, Singla, Longlai, Madhura, Sonai, Rukni, and Katakhal are the main tributaries of Barak, and they are all located in India. The whole basin includes portions of Myanmar, Bangladesh, and India. It covers a large portion of Assam, Nagaland, Meghalaya, Manipur, and Mizoram in India. With a total size of 41,723 km<sup>2</sup>, the Barak River Basin constitutes about 1.38 percent of India's landmass. Up to Badarpurghat, India (92.58°E, 24.87°N), a region of about 25,000 km<sup>2</sup> is taken into account in this research. There are low-lying, waterlogged regions, plains, and hills in this area's topography.

From December to February, the winter season typically begins and ends with rather dry weather. Precipitation in the winter is brought on by disturbances in the west, but in the months leading up to the monsoon, thunderstorms and severe storms in the area bring hail and strong winds. Low, variable rainfall with the odd hailstorm is typical in the months of March and April as well as October and November. A lot of thunderstorms happen in May before the monsoon starts because moisture from the nearby Bay of Bengal makes its way into the area. Extreme precipitation and the threat

of flooding are hallmarks of the months of May through September. In spite of a respectable annual total, the seasonal distribution reveals a highly erratic pattern with the highest precipitation occurring between June and August. The Barak basin is prone to devastating floods because of the heavy rainfall that occurs there during the monsoon season. The climate in the Barak Basin is subtropical, warm, and humid. The annual rainfall ranges between 2,500 to 4,000 mm. The average annual rainfall in the Barak basin of Assam declined by 34.0 mm per decade between 1901 and 2010. Trend analysis including multiple climatic normal periods shows that the basin's annual total rainfall declined dramatically over the past 30 years (1981–2010). During this time, the rainfall in the Barak basin decreased by 315.3 mm per decade, as reported by Deka et al. (2012). The temperature is very constant throughout the year, with January typically averaging 12.2°C and August 25.4°C, and January reaching an average high of 24.3°C and August 36.0°C. Figure 3.2 depicts the research region, whereas Figure 3.1 displays the Barak and adjacent basins.

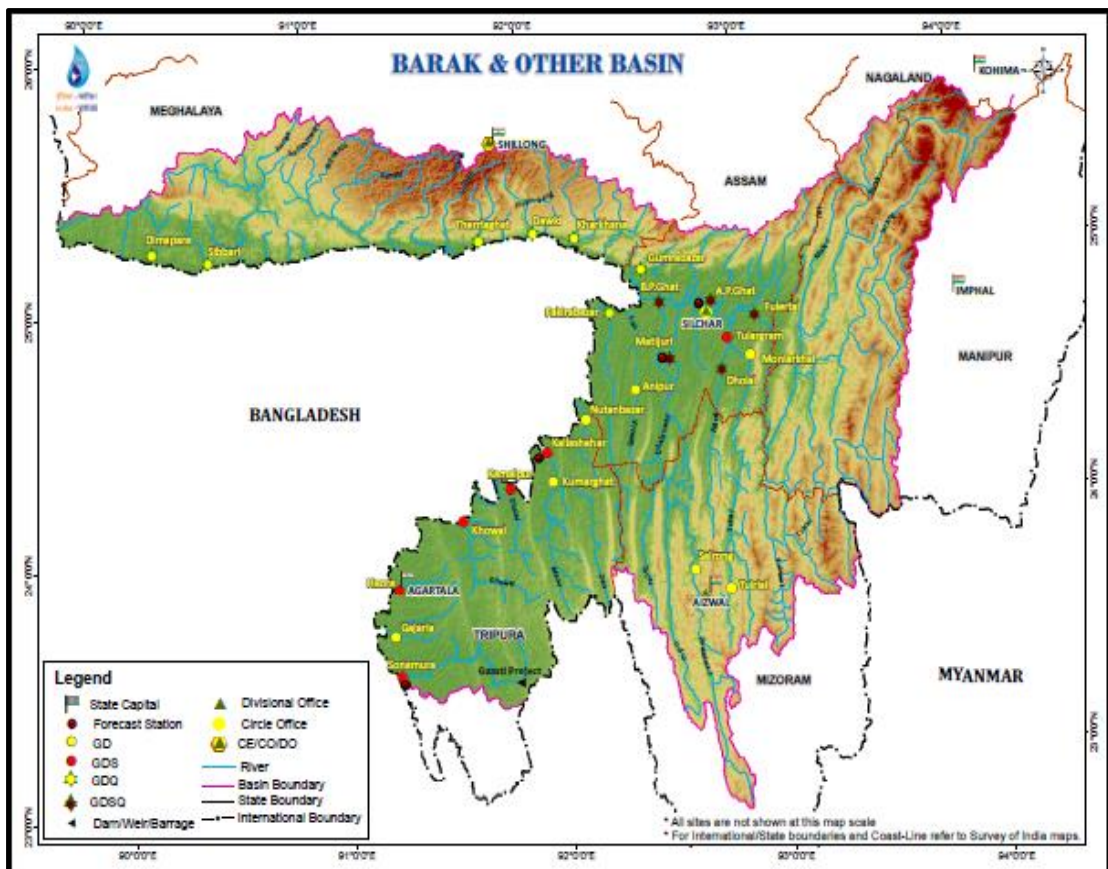


**FIGURE 3.1** Barak and other basins (Source India WRIS)

### 3.1.1 SALIENT FEATURES OF BARAK AND OTHER BASINS

#### Full Basin Extent

Longitude	89°50' to 94°0'E
Latitude	22°44' to 25°58' N
Length of Barak River (Kms)	564 (in India)
Catchment Area (Sq. Kms)	41723(1.38% of the total geographical area of the country)

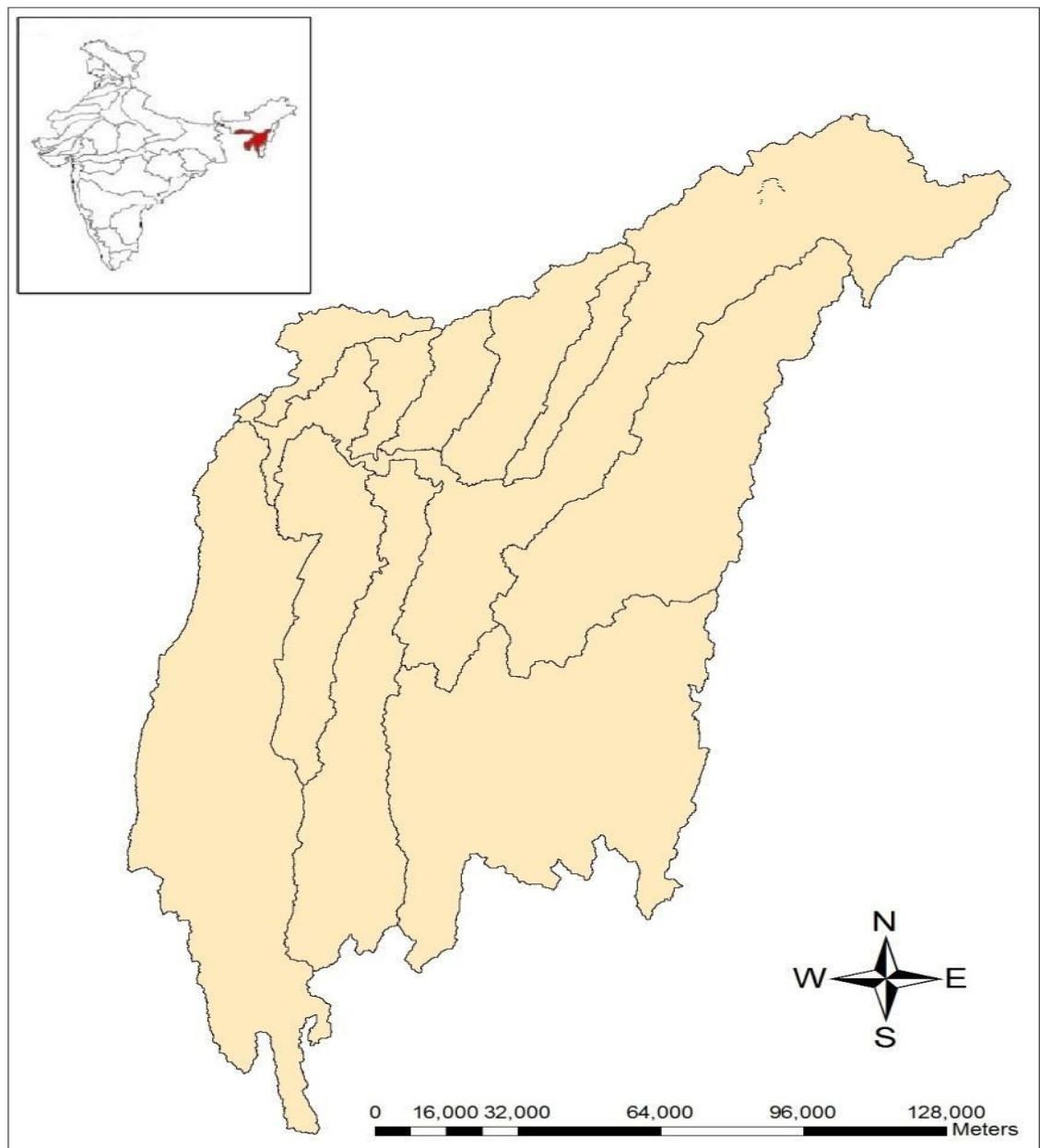


**FIGURE 3.2** Location map of study area

### 3.2 DATABASE

All of the gauging stations' daily rainfall amounts are essential for the investigation. Unfortunately, the data used to construct IDF correlations are sometimes lacking or insufficiently distributed because to a lack of rain gauge stations, which is a prevalent issue in poor nations. Therefore, this research makes advantage of Global Weather Data. If you want to get your hands on them, you may do it by downloading the data sets from the Global Weather Data for SWAT portal. In order to construct the IDF curves for the current climate, we make use of thirty years of data (1979–2009) and thirty years of daily precipitation data (1979–2013) from twenty-three stations in the study area retrieved from [www.globalweather.tamu.edu](http://www.globalweather.tamu.edu). The study's selected stations are depicted in Figure 3.3.

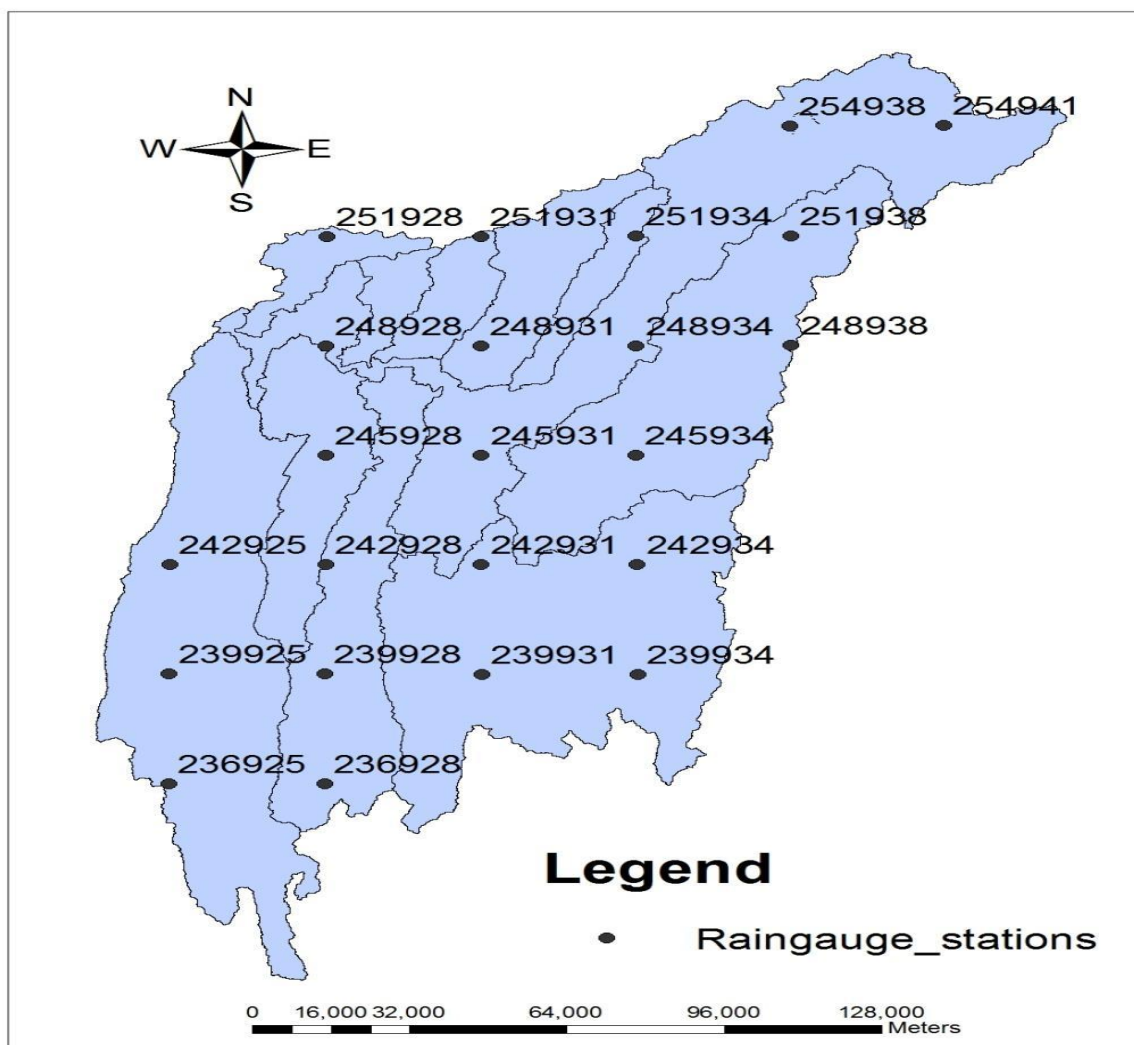


**FIGURE 3.3** Location of rain gauge stations used in the study

**Table 3.1:** Location of the Rain Gauge Stations

<b>STATION IDs</b>	<b>LOCATION OF THE RAIN GAUGE STATIONS</b>
236925	Chintuipui
236928	Tiawng
239925	Tiau
239928	Khawthiangtuipui
239931	Longai
239934	Dhaleswari
242925	Tuichawng
242928	Monu
242931	Sumil
242934	Nangmai
245928	Tuivai
245931	Sonai
245934	Nambel
248928	Kongphung
248931	Barak
248934	Kushiyara
248938	Iril
251928	Jiri
251931	Kopili
251934	Myntdu
251938	Doyang
254938	Chiri
254941	Chathe

The data for the digital elevation model used to extract the basin was obtained from the following website: <http://gdex.cr.usgs.gov/>. For the same region, we used the CCISC data site to get SDSM predictors. For the specified geographic coordinates of the closest grid box to the research region, the available GCM (HadCM3) was used as a predictor. The next step in deploying SDSM was to download all of the data files directly.

# CHAPTER 4

## METHODOLOGY

---

---

### 4.1 INTRODUCTION

In this chapter, different methods and processes used in the research is included. An overview has been prepared of the methods as given below.

### 4.2 DATA PRE-PROCESSING

Daily precipitation data at 23 stations in the research region are retrieved from [www.globalweather.tamu.edu](http://www.globalweather.tamu.edu) over a 35-year period (1979-2013) in order to generate IDF curves. Data on daily precipitation was broken down into smaller intervals of 30 min, 1, 2, 3, 6, 12, and 24 hours. The precipitation data at each station was tested for consistency of the rain gauge stations.

#### 4.2.1 DAILY RAINFALL DISAGGREGATION METHOD

After obtaining the AMS from the daily precipitation record, we separated it into shorter-term rainfall series using the Indian Meteorological Department's (IMD) one-third reduction approach in equation (1). The best effective formula for calculating short-duration rainfall for Sylhet city was discovered to be the IMD one-third reduction method by Chowdhury et al. (2007). (Rashid et al., 2012).

$$p_t = p_{24} \left( \frac{t}{24} \right)^{1/3} \quad (4.1)$$

where  $p_t$  stands for the millimetre-scale rainfall depth over t-hours,  $p_{24}$  for the millimetre-scale rainfall over a 24-hour period, and t for the hour-scale rainfall duration during which the depth measurement is needed. In order to analyse the rainfall occurrences, the AMS was divided into shorter intervals of 30, 1, 2, 3, 6, 12, and 24 hours.

#### **4.2.2 CONSISTENCY ANALYSIS**

There has been preliminary examination of the precipitation data in each to ensure consistency of the rain gauge. The double mass curve, primarily utilised to rectify the precipitation record, has been used for this purpose. When plotting the base station's cumulative rainfall against the average rainfall of surrounding stations, we can see if the lines are straight and if the variables are correlated.

### **4.3 BUILDING CLIMATE CHANGE SCENARIOS**

#### **4.3.1 GENERAL CIRCULATION MODEL (GCM)**

The Hadley Centre for Climate Prediction and Research in England's HadCM3 was one of the GCM models used in this investigation. In order to minimise uncertainties, it is suggested that you use an ensemble of GCM model outputs; unfortunately, time constraints meant that only HadCM3's output could be used in this research. Two causes led to the model's adoption. For starters, the model constituted the backbone of the majority of impact research on climate change. Secondly, it supplies Statistical Downscaling Model (SDSM) candidates in the form of large-scale daily predictor variables (Wilby and Dawson, 2007).

#### **4.3.2 CLIMATE CHANGE SCENARIOS**

These future scenarios were built using the HadCM3 model's output from the A2 (medium-high emissions) and B2 (medium-low emissions) scenarios. Based on the present climate, we divided the future timelines into two parts: (2011–2030) and (2031–2050).

#### **4.3.3 STATISTICAL DOWNSCALING MODEL (SDSM) PROCEDURES**

SDSM establishes a statistical relationship between predictor and predictand to downscale future climate conditions. Predictor variables give daily data on the large-scale meteorological condition, whereas predictand variables characterise the situation at the site scale. We used the SDSM software for:

1. Data Quality Control
2. Screening of Predictor variables
3. Model Calibration
4. Weather Generation
5. Statistical Analysis

6. Graphing Model Outputs
7. Scenario Generation

#### 4.4 INTENSITY-DURATION-FREQUENCY ANALYSIS

To begin the intensity duration frequency study, daily precipitation data was collected. We retrieved the yearly maximum from the records after we obtained the precipitation data. To estimate rainfall amounts for desired return periods, the yearly maximum data was fitted to probability distribution functions.

##### 4.4.1 FITTING THE PROBABILITY DISTRIBUTION

The maximum rainfall data series for 1, 2, 3, 6, 12, and 24 hours were analysed using frequency analysis to determine which distribution function would be best for computing these events over the desired return periods. Using the Gumbel, Lognormal, and Log Pearson Type III distributions, the data series were ordered in decreasing magnitude. This was achieved by testing the R-squared value for each station and duration using the Weibull plotting position techniques. The maximum annual rainfall data was then displayed against the probability distribution function, which comprised the reduced variate ( $Y_T$ ) in the Gumbel case, the standard normal variable ( $Z$ ) in the Lognormal case, and the frequency factor ( $K_T$ ) in the Log Pearson Type III case. The maximum rainfall data for each year was fitted to the Gumbel, Lognormal, and Log Pearson Type III probability distributions using this approach. Positions plotted using the Weibull technique were utilised.

**Log Normal Distribution:** The frequency factor  $K_T$  is equal to  $Z$  for the distribution and given by:

$$Z = w - \frac{2.515517 + 0.802853w + 0.010328w^2}{1 + 1.432788w + 0.189269w^2 + 0.001308w^3} \quad (1.3)$$

$$\text{here,} \quad w = \sqrt{\frac{1}{p^2}} \quad (0 < p \leq 0.5) \quad (1.4)$$

$P$  is the probability of exceedance. When  $p > 0.5$ ,  $1-p$  is substituted in (1.3).

**Gumbel Distribution:** The frequency distribution in hydrological investigations is often represented by the Gumbel distribution. A two-parameter distribution, the

Gumbel distribution goes by many names than just that. The Gumbel distribution's frequency factor is expressed as:

$$K_T = \frac{\sqrt{6}}{\pi} \left( 0.5772 + \ln \left( \ln \left( \frac{T}{T-1} \right) \right) \right) \quad (1.5)$$

**Log Pearson Type III:** There are three components that make up the LPT III frequency distribution. The mean, the slope of the straight line for standard deviation, and the degree of curvature for skewness coefficient are all used in probability theory to indicate the average ordinate, standard deviation, and skewness, respectively. Logarithms of the predicted values are used in the distribution. We may get the skewness coefficient,  $C_s$ , using equation (1.8). To get the distribution's frequency factor, one must know the skewness coefficient.

$$\overline{\log x} = \frac{\sum \log x}{n} \quad (1.6)$$

$$\sigma_{\log x} = \sqrt{\frac{\sum (\log x - \overline{\log x})^2}{n-1}} \quad (1.7)$$

$$C_s = \frac{n \sum (\log x - \overline{\log x})^3}{(n-1)(n-2)(\sigma_{\log x})^3} \quad (1.8)$$

The value of  $x$  for a specified return period is computed as given in (1.9):

$$\log x = \overline{\log x} + K_T \sigma_{\log x} \quad (1.9)$$

The frequency factor,  $K_T$ , is dependent on the skewness coefficient,  $C_s$ , and the return period,  $T$ . Numerous references on water resources may be used to determine the frequency factor values (Chow et al., 1988) or they can be computed as:

$$K_T = Z + (Z^2 - 1)K + \frac{1}{3}(Z^3 - 6Z)K^2 - (Z^2 - 1)K^2 + ZK^4 + \frac{1}{3}K^5 \quad (1.9)$$

where, 
$$K = \frac{C_s}{6} \quad (1.10)$$

#### 4.4.2 TESTING THE GOODNESS OF FIT OF DATA

Tests for goodness of fit (GOF) determine if a random sample follows a theoretical probability distribution function. To rephrase, these tests show how well the selected distribution fits the data. If you want to choose a distribution to characterise the rainfall series and accurately predict when a storm will occur, you must find the best frequency analysis approach. To select the optimal model, EasyFit software is utilised in conjunction with the three most common GOF tests, which are the Kolmogorov-Smirnov (K-S), Anderson-Darling (A-D), and Chi-Squared ( $\chi^2$ ) tests (Subyani & Al-Amri, 2015). Specifically, these tests determine if a particular distribution is a good match by computing test-statistics. It is in Table 4.1 that the test data are detailed. According to Sharma et al. (2016), while estimating the parameters, the EasyFit programme uses the Maximum Likelihood Method for the LN distribution and the Method of Moments for the Gumbel and LPIII distributions. We calculate the test statistics and then sort the probability distributions by their lowest values.

**Table 4.1** Description of goodness-of-fit tests (Sharma et al. 2012)

GOF TEST	TEST STATISTIC
Kolmogorov-Smirnov (K-S) test	$D = \max  P(X_m) - F(X_m) $ <p>where, <math>P(X_m)</math> is the cumulative probability distribution for each of the ordered observations <math>X_m</math> using Weibull's formula, and <math>F(X_m)</math> is the theoretical cumulative probability for each of the ordered observations <math>X_m</math> using the assumed distribution.</p>
Anderson-Darling (A-D) test	$A^2 = -n - S$ $S = \sum \frac{2k-1}{n} [\ln F(Y_k) + \ln \{1 - F(Y_{n+1-k})\}]$ <p>where, <math>Y_1, Y_2, \dots, Y_n</math>=data series, <math>F</math>=cumulative distribution function (CDF), and <math>n</math>=size of the sample.</p>

Chi-Squared ( $\chi^2$ ) test	$\chi^2 = \sum_{i=1}^k \frac{(O_i - E_i)^2}{E_i}$ <p>Where, <math>O_i</math>= observed frequency for class <math>i</math>, and <math>E_i</math>= expected frequency for the class <math>i</math>.</p>
-------------------------------	---

#### 4.4.3 COMPUTATION OF EXTREME VALUES ( $X_T$ )

The quantiles of extreme rainfall occurrences were determined for each station and rainfall durations of 30, 1, 2, 3, 6, 12, and 24 hours using LPT III. The return periods were 2, 5, 10, 25, 50, and 100 years, as shown in (1.2). Rainfall durations and frequencies stated above were chosen for the most part because they are routinely used in the construction of various hydraulic systems.

#### 4.4.4 CALCULATING INTENSITY OF RAINFALL (I)

The rainfall intensity is expressed using equation (4.17):

$$I = \frac{R}{T_d} \quad (4.17)$$

where R is the rainfall measured in millimetres and  $T_d$  is the period measured in hours. With the  $X_T$  data in hand, we can calculate the rainfall intensities for a certain duration ( $D_i$ ) and a set of return periods ( $T_r$ ).

### 4.5 DERIVATION OF IDF EQUATION

The outcomes from the IDF curves are the primary data points for determining the necessary steps to derive an equation that can be used to calculate the rainfall intensity (I) for the areas of interest, given a specific recurrence interval and rainfall period. In order to find all of the parameters associated with an equation, one may use the logarithmic conversion to transform it into a linear equation (Elsebaie, 2011). The following steps are followed:

1. Convert the original equation in the form of power-law relation as follows:

$$I = \frac{CT_r^m}{T_d^e} \quad (4.18)$$

By applying the logarithmic function to get

$$\log I = \log K - e \log T_d \quad (4.19)$$

where, 
$$K = CT_r^m \quad (4.20)$$

And  $e$  represents the slope of the straight line.

2. Calculate the natural logarithm for ( $K$ ) value found from the probability distribution method as well as the natural logarithm for return period  $T_d$ .
3. Plot the values of ( $\log I$ ) on the y-axis and the value of ( $\log T_d$ ) on the x-axis for all the return periods.
4. From the graphs (or mathematically) find the value of ( $e$ ) for all return periods. Then find the average value of  $e$ ,  $e_{avg}$  by using the following equation:

$$e_{avg} = \frac{\sum e}{n} \quad (4.21)$$

Where  $n$  represents the number of return periods noted as  $T_r$ .

5. From the graph, find  $\log K$  values for each recurrence interval where  $\log K$  represents the y-intercept values. Then convert (4.20) into a linear equation by applying the natural logarithm to become:

$$\log K = \log C + m \log T_r \quad (4.22)$$

6. Plot the values of  $\log K$  on the y-axis and the values of  $\log T_r$  on the x-axis to find out the values of parameters  $C$ ,  $m$  and  $e$  where  $m$  represents the slope of the straight line and  $C$  represents the antilog for the y-intercept.

## 4.6 DEVELOPING ISOPLUVIAL MAPS

We calculate the maximum rainfall intensity for each station for various return times for particular durations. The developed rainfall intensity maps of Isopluvial are used to estimate this intensity of rainfall for ungauged sites (Gebreslassie, 2014). Isopluvial maps were developed to show the spatial variability of rainfall intensities in the basin.

To create Isopluvial maps for a certain time period over the whole basin, Arc-GIS is used in conjunction with the Inverse Distance Weighting technique to interpolate the values of rainfall intensity ( $I$ ) from various stations to the ungauged locations. (Sarkar et al., 2012).

#### 4.7 COMPARISON OF INTENSITY DURATION FREQUENCY RESULTS

A comparison was made between an IDF curve that was created using historical observed data for the stations and one that was constructed under climate change scenarios (rainfall intensity). The following relationship was used to obtain the relative differences (RD) between the curves. (Prodanovic and Simonovic, 2007):

$$relativedifference = \frac{X_1 - X_2}{\left(\frac{X_1 + X_2}{2}\right)} \times 100 \quad (4.23)$$

Rainfall intensity under current climatic conditions is denoted by  $X_2$ , whereas rainfall intensity during climate change is represented by  $X_1$ . There may be important implications for the design, operation, and maintenance of future and existing water management facilities arising from the discrepancy between the two IDF curves.

# CHAPTER 5

## RESULTS AND DISCUSSIONS

---

---

### 5.1 INTRODUCTION

The results obtained in the study are shown below in tabular format along with the graphical format for each of the A2 and B2 scenarios along with the current climate scenario.

### 5.2 CONSISTENCY OF THE RAINFALL DATA SERIES

Over the time period under consideration, the rainfall data remained consistent, as indicated by the nearly linear graph of the double mass curve plot, which is the plot of the cumulative annual rainfall data of the base station with the cumulative average annual rainfall data of neighbourhood stations of the stations under consideration. The coefficient of determination ( $R^2$ ) ranged from 0.996-0.999.

### 5.3 CLIMATE CHANGE SCENARIOS OF RAINFALL

This section is a discussion of the future of climate change scenarios, the model's performance assessment, the predictor variables that were chosen for investigation, and the statistics used for calibration and validation.

#### 5.3.1 SELECTED ATMOSPHERIC PREDICTOR VARIABLES

The twenty-six predictor variables included in the NCEP reanalysis data sets for future climate change scenario outputs were selected for calibration and creation based on their ability to create a greater partial correlation ( $r$  at  $p < 0.05$ ) with the predictand variable. Table 5.1 displays the variables that were selected.

**Table 5.1** Selected predictor variables

Predictor Variables	Predictors Description
Tempas	Temperature

r850	relative humidity at 850 hpa
r500	relative humidity at 500 hpa
p5_uas	zonal velocity at 500 hpa
p5_vas	meridional velocity at 500 hpa
p850	geopotential height at 850hpa
Rhum	near surface relative humidity
Shum	surface specific humidity

The partial correlation coefficient( $r$ ) shows the explanatory power that is specific to each predictor. hPa is a unit of pressure, 1 hPa = 1 mbar = 100 Pa = 0.1 kPa.

Scatter plots and partial correlation values among the 26 reanalysis NCEP predictor factors were used to choose the predictor variables. Therefore, the study's predictor variables were determined to be reasonable based on the data in the table.

### 5.3.2 CALIBRATION AND VALIDATION OF THE MODEL

Table 5.2 displays the calibration statistics for the predictand variable, which is rainfall. The regression model is calibrated using 13 years of data (1979–2001), and validated using 8 years of data (2002–2009).

**Table 5.2** Performance of model during calibration period

Daily rainfall (mm)	R-squared	Standard Error
SDSM (Annual)	0.29	0.446
SDSM (Monthly)	0.476	0.427

**Table 5.3** Performance of model during validation period

Year	2002	2003	2004	2005	2006	2007	2008	2009
Annual Percentage Error	5.5	6.2	2.4	15.7	12.58	2.6	7.47	7.37

Tables 5.2 and 5.3 demonstrate that the model's performance is low throughout validation and calibration. Wilby and Dawson (2007), who created the SDSM, said that the predictors' estimated  $R^2$  ranged from 0.65 for temperatures between 60% and 85% and from 0.1 for precipitation levels over 10% (and sometimes below 10%). Low  $R^2$  values shouldn't discourage users, according to Wilby and Dawson (2007). Reason being, SDSM doesn't take into consideration local factors like land use, topography, etc., which impact precipitation, an intermediate process that is governed by the provided large-scale predictor variables. There is no cut off points set to reject from using the model based on  $R^2$  values. For that reason, in most of the literatures, the  $R^2$  values are hardly mentioned.

For the performance evaluation of the model, the observed values and the generated values of the base periods were calculated for a yearly time step and comparisons were made. It is noted that for the Barak Basin, the annual rainfall would increase by 31.19% and 42.38% during 2011-2030 and 33.38% and 45.6% during 2031-2050 under H3A2 and H3B2, respectively. But there's a noticeable drop in the maximum daily rainfall. This proves that SDSM isn't very good at simulating very high or low rainfall levels. Souvignet (2010) noted that while linear trends and extreme events had their maximum and minimum temperatures accurately simulated, precipitation simulations produced weaker results, and that SDSM was not a very robust method for simulating precipitation. The finding is deemed appropriate, nevertheless, since precipitation is inherently conditional, meaning that some intermediate state variable controls the link between the predictors and predictants.

#### **5.4 GENERATION OF IDF CURVES**

The precipitation data was used to determine the IDF curves at each station in order to create the curves using historical data. To get average IDF curves for the whole basin, the Thiessen Polygon technique was used.

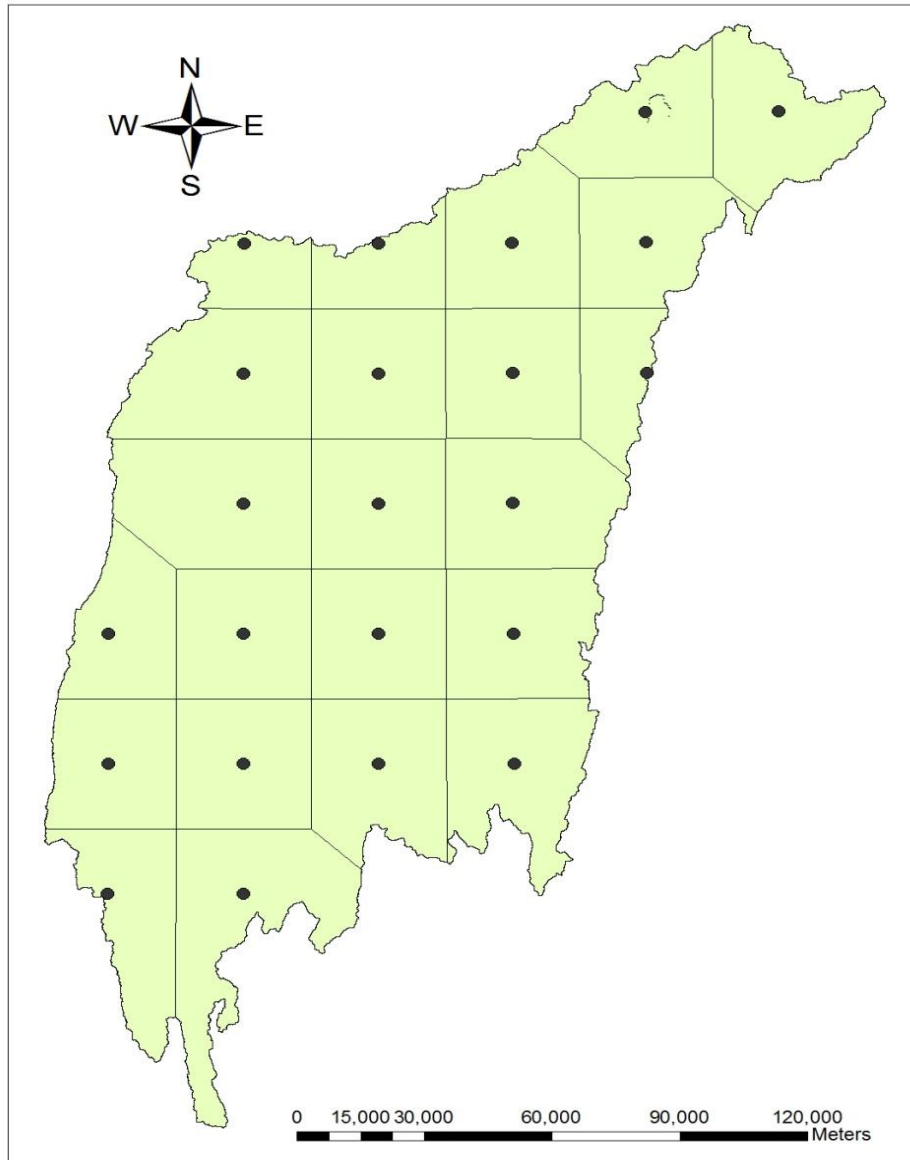


**Figure 5.1** Thiessen Polygon map of the study area

For IDF curves under future scenario, an average of daily precipitation of all the stations was taken using Thiessen Polygon method and then was put into SDSM for finding the precipitation under changing climate scenario. Figure 5.1 shows the Thiessen Polygons created in the research region using ArcGIS.

#### **5.4.1 DISAGGREGATION OF DAILY RAINFALL**

We used the historical data to create daily rainfall scenarios using SDSM. Then, we used the IMD empirical reduction technique to extract the yearly maximum and break it down into the needed sub-daily rainfall at different time intervals: 30 minutes, 1 hour, 2 hours, 3 hours, 6 hours, 12 hours, and 24 hours.

#### 5.4.2 SELECTION OF BEST FITTING PROBABILITY DISTRIBUTION FUNCTION

The most popular probability distributions used in hydrological studies, including the Gumbel, Log normal, and Log Pearson type III distributions, were compared in order to determine the best match for computing extreme rainfall values ( $X_T$ ) for certain durations. Table 5.4 displays the values of the coefficient of determination ( $R^2$ ).

**Table 5.4 R-Squared Values for AMS**

Station ID	Type of Distribution	24hr	Rank
248928	Gumbel Extreme Value I	0.947	2
	Log normal	0.903	3
	<b>Log Pearson type III</b>	<b>0.953</b>	<b>1</b>
248931	Gumbel Extreme Value I	0.941	2
	Log normal	0.88	3
	<b>Log Pearson type III</b>	<b>0.946</b>	<b>1</b>
245928	Gumbel Extreme Value I	0.921	2
	Log normal	0.844	3
	<b>Log Pearson type III</b>	<b>0.929</b>	<b>1</b>
245931	Gumbel Extreme Value I	0.975	2
	Log normal	0.965	3
	<b>Log Pearson type III</b>	<b>0.981</b>	<b>1</b>
242925	Gumbel Extreme Value I	0.935	2
	Log normal	0.837	3
	<b>Log Pearson type III</b>	<b>0.958</b>	<b>1</b>
242928	Gumbel Extreme Value I	0.919	2
	Log normal	0.837	3
	<b>Log Pearson type III</b>	<b>0.933</b>	<b>1</b>
239925	Gumbel Extreme Value I	0.883	2
	Log normal	0.761	3
	<b>Log Pearson type III</b>	<b>0.931</b>	<b>1</b>
239928	Gumbel Extreme Value I	0.92	2
	Log normal	0.826	3
	<b>Log Pearson type III</b>	<b>0.936</b>	<b>1</b>
236925	Gumbel Extreme Value I	0.969	2
	Log normal	0.905	3
	<b>Log Pearson type III</b>	<b>0.974</b>	<b>1</b>
236928	Gumbel Extreme Value I	0.99	1
	Log normal	0.974	2
	<b>Log Pearson type III</b>	<b>0.991</b>	<b>1</b>
242931	<b>Gumbel Extreme Value I</b>	<b>0.971</b>	<b>1</b>
	Log normal	0.952	3

	Log Pearson type III	0.975	2
242934	<b>Gumbel Extreme Value I</b>	<b>0.952</b>	<b>1</b>
	Log normal	0.913	3
	Log Pearson type III	0.947	2
245934	Gumbel Extreme Value I	0.971	3
	Log normal	0.979	2
	<b>Log Pearson type III</b>	<b>0.981</b>	<b>1</b>
248934	Gumbel Extreme Value I	0.973	2
	Log normal	0.91	3
	<b>Log Pearson type III</b>	<b>0.975</b>	<b>1</b>
248938	Gumbel Extreme Value I	0.981	2
	Log normal	0.971	3
	<b>Log Pearson type III</b>	<b>0.982</b>	<b>1</b>
239931	Gumbel Extreme Value I	0.873	2
	Log normal	0.795	3
	<b>Log Pearson type III</b>	<b>0.897</b>	<b>1</b>
239934	Gumbel Extreme Value I	0.962	2
	Log normal	0.908	3
	<b>Log Pearson type III</b>	<b>0.964</b>	<b>1</b>
251928	<b>Gumbel Extreme Value I</b>	<b>0.988</b>	<b>1</b>
	Log normal	0.963	3
	Log Pearson type III	0.985	2
251931	Gumbel Extreme Value I	0.985	2
	Log normal	0.953	3
	<b>Log Pearson type III</b>	<b>0.987</b>	<b>1</b>
251934	Gumbel Extreme Value I	0.968	2
	Log normal	0.891	3
	<b>Log Pearson type III</b>	<b>0.971</b>	<b>1</b>
251938	Gumbel Extreme Value I	0.978	2
	Log normal	0.922	3
	<b>Log Pearson type III</b>	<b>0.982</b>	<b>1</b>
245938	Gumbel Extreme Value I	0.989	2
	Log normal	0.941	3
	<b>Log Pearson type III</b>	<b>0.991</b>	<b>1</b>
245941	Gumbel Extreme Value I	0.985	2
	Log normal	0.934	3
	<b>Log Pearson type III</b>	<b>0.981</b>	<b>1</b>

The level of agreement between the simulated and measured values is greater when  $R^2$  is near to 1. The three probability distributions were considered, and the Log Pearson Type III distribution was chosen based on  $R^2$  values.

### 5.4.3 GOODNESS OF FIT OF DATA

After the R-squared test for distribution selection, we checked the data's goodness of fit to the probability distribution function for all durations' maximum yearly rainfall values. We used this test to ensure that the Log Pearson Type III probability distribution was suitable. The GOF tests that used the Anderson-Darling, Chi-squared, and Kolmogorov-Smirnov tests were conducted using Easy Fit software version 5.6. Table 5.5 displays the tabulated results of the Goodness of fit test, which demonstrate that the chosen distribution is suitable and can match the statistical data used for the study.

**Table 5.5** Goodness of fit for Log Pearson Type III distribution for station 242928

<b>Log Pearson Type III</b>					
<b>Kolmogorov-Smirnov</b>					
Statistic	0.1104				
P-Value	0.7463				
$\alpha$	0.2	0.1	0.05	0.02	0.01
Critical Value	0.17659	0.20185	0.22425	0.25073	0.26897
Reject?	No	No	No	No	No
<b>Anderson-Darling</b>					
Statistic	0.4166				
$\alpha$	0.2	0.1	0.05	0.02	0.01
Critical Value	1.3749	1.9286	2.5018	3.2892	3.9074
Reject?	No	No	No	No	No
<b>Chi-Squared</b>					
Deg. of freedom	3				
Statistic	0.0353				
P-Value	0.9983				
$\alpha$	0.2	0.1	0.05	0.02	0.01
Critical Value	4.6416	6.2514	7.8147	9.8374	11.345
Reject?	No	No	No	No	No

The distribution associated with the station may be chosen as the best fit distribution if the P-value is greater than  $\alpha$ , as stated in the test principle (Chow, 1988). At the selected significance level ( $\alpha$ ) = 0.05, if the test statistic is higher than the critical value derived from a table, the hypothesis about the distributional form is rejected. Typically, while evaluating the null hypothesis ( $H_0$ ) at different significance levels, the fixed values of

0.05 are used. For this reason, the maximum yearly rainfall was determined to be consistent with the Log Pearson Type III distribution.

#### 5.4.4 COMPUTED EXTREME RAINFALL QUANTILES ( $X_T$ )

As a whole, Tables 5.3–5.6 summarise the calculated rainfall quantiles for certain time periods and return periods based on the basin's historic (1979–2013) and downscaled A2 and B2 climate scenario data for the (2011–2030) and (2031–2050) time horizons, respectively. Tables 5.7–5.11 demonstrate that for all future time lines, the calculated quantiles of rainfall under the A2 climate scenario were lower. Additionally, the time horizon in the B2 scenario will result in a reduction.

**Table 5.6** Computed rainfall quantiles  $X_T$  (mm) using historic data of current climate for different return periods and durations

Duration (hr)	Return Period (year)					
	2	5	10	25	50	100
0.5	33.95	45.09	52.85	63.13	71.18	79.41
1	42.73	56.80	66.63	79.72	90.00	100.55
2	53.84	71.56	83.95	100.44	115.17	126.67
3	61.63	81.92	96.10	114.98	131.65	145.01
6	77.65	103.21	121.08	144.86	167.95	182.71
12	97.95	130.18	152.71	182.70	206.25	230.41
24	123.26	161.50	189.55	226.93	256.31	286.47

**Table 5.7** Computed rainfall quantiles  $X_T$  (mm) using A2 scenario data of 2011-2030 for different return periods and durations

Duration (hr)	Return Period (years)					
	2	5	10	25	50	100
0.5	8.00	8.55	8.88	9.26	9.53	9.79
1	10.08	10.77	11.19	11.68	12.02	12.34
2	12.70	13.57	14.10	14.71	15.14	15.55
3	14.54	15.54	16.14	16.84	17.33	17.80
6	18.32	19.58	20.33	21.22	21.83	22.43
12	23.08	24.67	25.62	26.73	27.51	28.25
24	29.08	31.08	32.28	33.68	34.66	35.60

**Table 5.8** Computed rainfall quantiles  $X_T$  (mm) using B2 scenario data of 2011-2030 for different return periods and durations

Duration (hr)	Return Period (years)					
	2	5	10	25	50	100
0.5	12.68	14.10	14.94	15.88	16.52	17.12
1	15.79	17.87	19.12	20.54	21.51	22.44
2	19.89	22.51	24.09	25.88	27.10	28.27
3	22.77	25.77	27.57	29.63	31.03	32.36
6	28.69	32.47	34.74	37.33	39.09	40.77
12	36.15	40.91	43.77	47.03	49.25	51.36
24	45.54	51.54	55.15	59.26	62.05	64.71

**Table 5.9** Computed rainfall quantiles  $X_T$  (mm) using A2 scenario data of 2031-2050 for different return periods and durations

Duration (hr)	Return Period (years)					
	2	5	10	25	50	100
0.5	7.93	8.39	8.66	8.97	9.18	9.39
1	9.99	10.57	10.91	11.30	11.57	11.83
2	12.58	13.31	13.74	14.23	14.58	14.90
3	14.40	15.24	15.73	16.29	16.69	17.06
6	18.15	19.20	19.82	20.53	21.03	21.50
12	22.87	24.19	24.97	25.87	26.49	27.08
24	28.81	30.48	31.46	32.59	33.38	34.12

**Table 5.10** Computed rainfall quantiles  $X_T$  (mm) using B2 scenario data of 2031-2050 for different return periods and durations

Duration (hr)	Return Period (years)					
	2	5	10	25	50	100
0.5	12.67	14.00	14.81	15.78	16.47	17.14
1	15.97	17.64	18.66	19.88	20.76	21.60
2	20.12	22.22	23.51	25.05	26.15	27.21
3	23.03	25.44	26.91	28.68	29.94	31.15
6	29.02	32.05	33.91	36.13	37.72	39.25
12	36.56	40.38	42.72	45.52	47.52	49.45
24	46.06	50.87	53.83	57.35	59.87	62.31

#### 5.4.5 COMPUTED RAINFALL INTENSITIES (I)

By dividing the estimated quantiles of the specified return periods by their respective lengths, we can determine the intensities for each station for both the historic and future climate change scenario data sets. The IDF curves that were derived from the various scenarios' rainfall intensities. Figure 5.2 shows the IDF curve for the basin using the historic data, Figure 5.3, 5.4, 5.5 and 5.6 shows the IDF curves under A2 scenario for (2011-30), B2 scenario for (2011-30), B2 scenario for (2031-2050) and B2 scenario for (2031-2050), respectively.

**Table 5.11** Computed intensity of rainfall, I (mm/hr) for current climate (1979-2013)

Duration (hr)	Return Period (year)					
	2	5	10	25	50	100
0.5	67.89	90.19	105.70	126.27	142.37	158.82
1	42.73	56.80	66.63	79.72	90.00	100.55
2	26.92	35.78	41.97	50.22	57.59	63.34
3	20.54	27.31	32.03	38.33	43.88	48.34
6	12.94	17.20	20.18	24.14	27.99	30.45
12	8.16	10.85	12.73	15.22	17.19	19.20
24	5.14	6.73	7.90	9.46	10.68	11.94

**Table 5.12** Computed intensity of rainfall, I (mm/hr) for A2 scenario (2011-2030)

Duration (hr)	Return Period (years)					
	2	5	10	25	50	100
0.5	16.00	17.10	17.76	18.53	19.07	19.58
1	10.08	10.77	11.19	11.68	12.02	12.34
2	6.35	6.79	7.05	7.35	7.57	7.77
3	4.85	5.18	5.38	5.61	5.78	5.93
6	3.05	3.26	3.39	3.54	3.64	3.74
12	1.92	2.06	2.13	2.23	2.29	2.35
24	1.21	1.29	1.34	1.40	1.44	1.48

**Table 5.13** Computed intensity of rainfall, I (mm/hr) for B2 scenario (2011-2030)

Duration (hr)	Return Period (years)					
	2	5	10	25	50	100
0.5	25.37	28.20	29.87	31.77	33.04	34.25
1	15.79	17.87	19.12	20.54	21.51	22.44
2	9.95	11.26	12.04	12.94	13.55	14.13
3	7.59	8.59	9.19	9.88	10.34	10.79
6	4.78	5.41	5.79	6.22	6.52	6.79
12	3.01	3.41	3.65	3.92	4.10	4.28
24	1.90	2.15	2.30	2.47	2.59	2.70

**Table 5.14** Computed intensity of rainfall, I (mm/hr) for A2 scenario (2031-2050)

Duration (hr)	Return Period (years)					
	2	5	10	25	50	100
0.5	15.85	16.77	17.31	17.93	18.37	18.78
1	9.99	10.57	10.91	11.30	11.57	11.83
2	6.29	6.66	6.87	7.12	7.29	7.45
3	4.80	5.08	5.24	5.43	5.56	5.69
6	3.02	3.20	3.30	3.42	3.50	3.58
12	1.91	2.02	2.08	2.16	2.21	2.26
24	1.20	1.27	1.31	1.36	1.39	1.42

**Table 5.15** Computed intensity of rainfall, I (mm/hr) for B2 scenario (2031-2050)

Duration (hr)	Return Period (years)					
	2	5	10	25	50	100
0.5	25.35	27.99	29.62	31.55	32.94	34.28
1	15.97	17.64	18.66	19.88	20.76	21.60
2	10.06	11.11	11.76	12.53	13.08	13.61
3	7.68	8.48	8.97	9.56	9.98	10.38
6	4.84	5.34	5.65	6.02	6.29	6.54
12	3.05	3.36	3.56	3.79	3.96	4.12
24	1.92	2.12	2.24	2.39	2.49	2.60

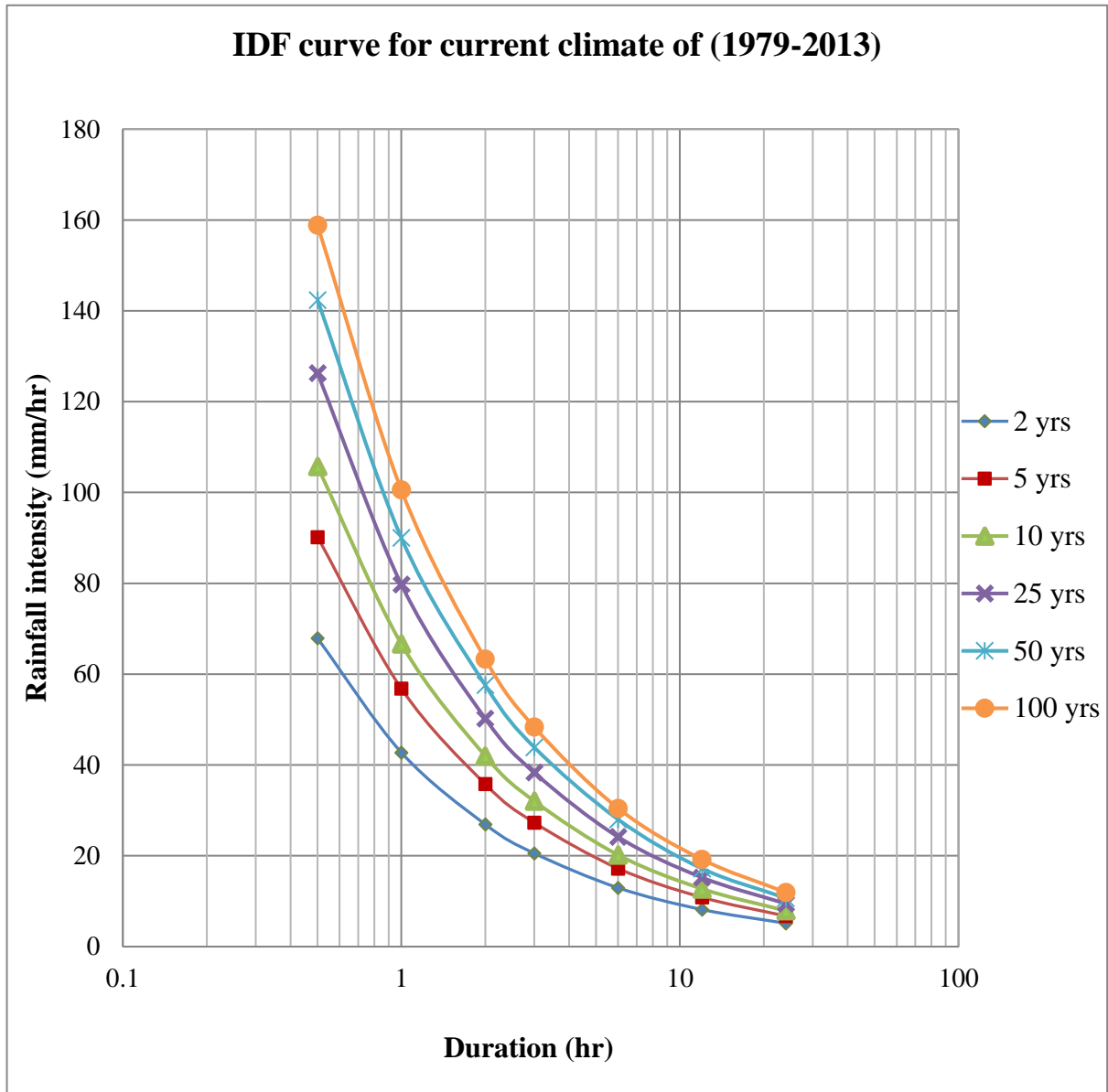


**Figure 5.2** IDF curve for current climate (1979-2013)

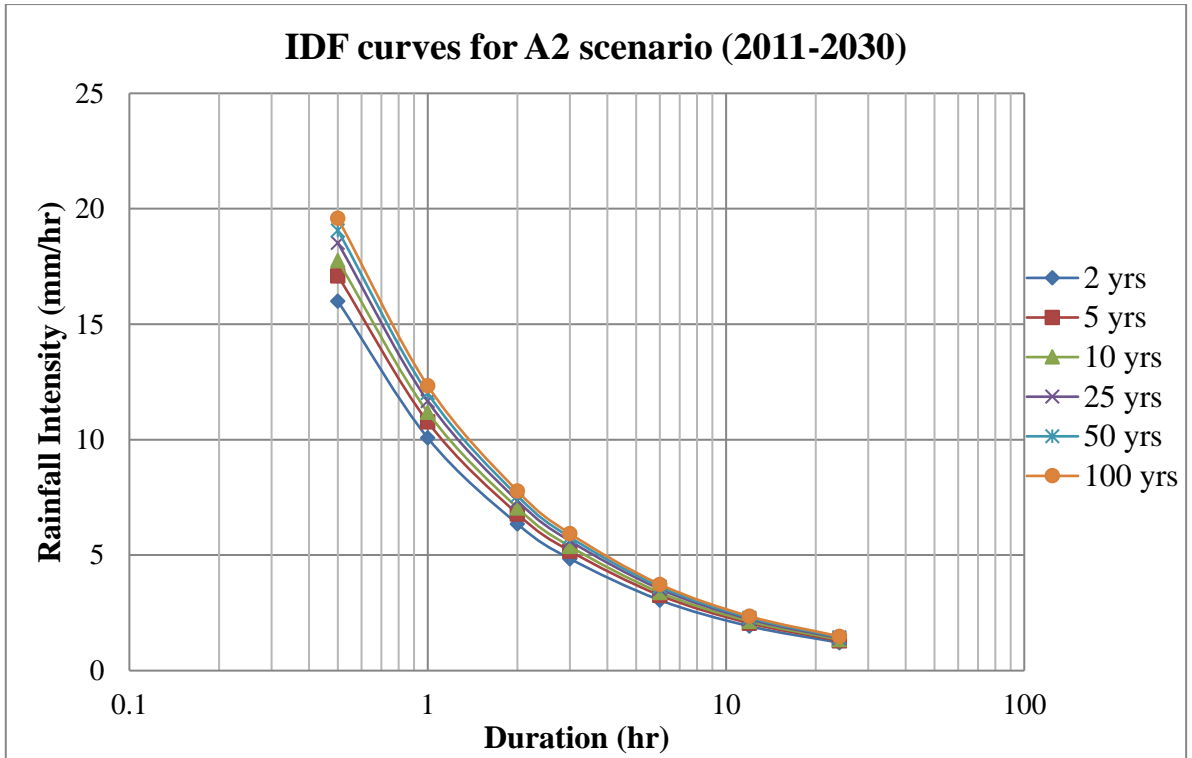


**Figure 5.3** IDF curve for A2 scenario (2011-2030)

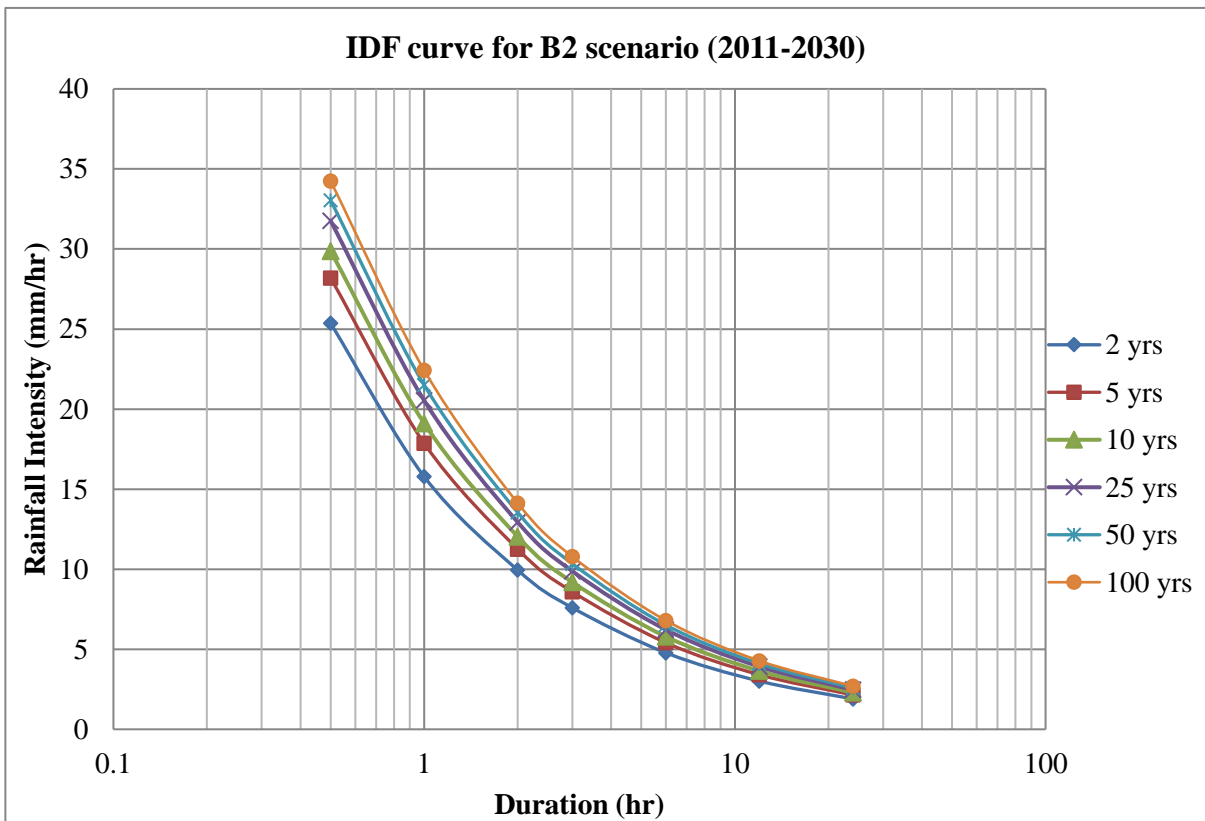


**Figure 5.4** IDF curve for B2 scenario (2011-2030)

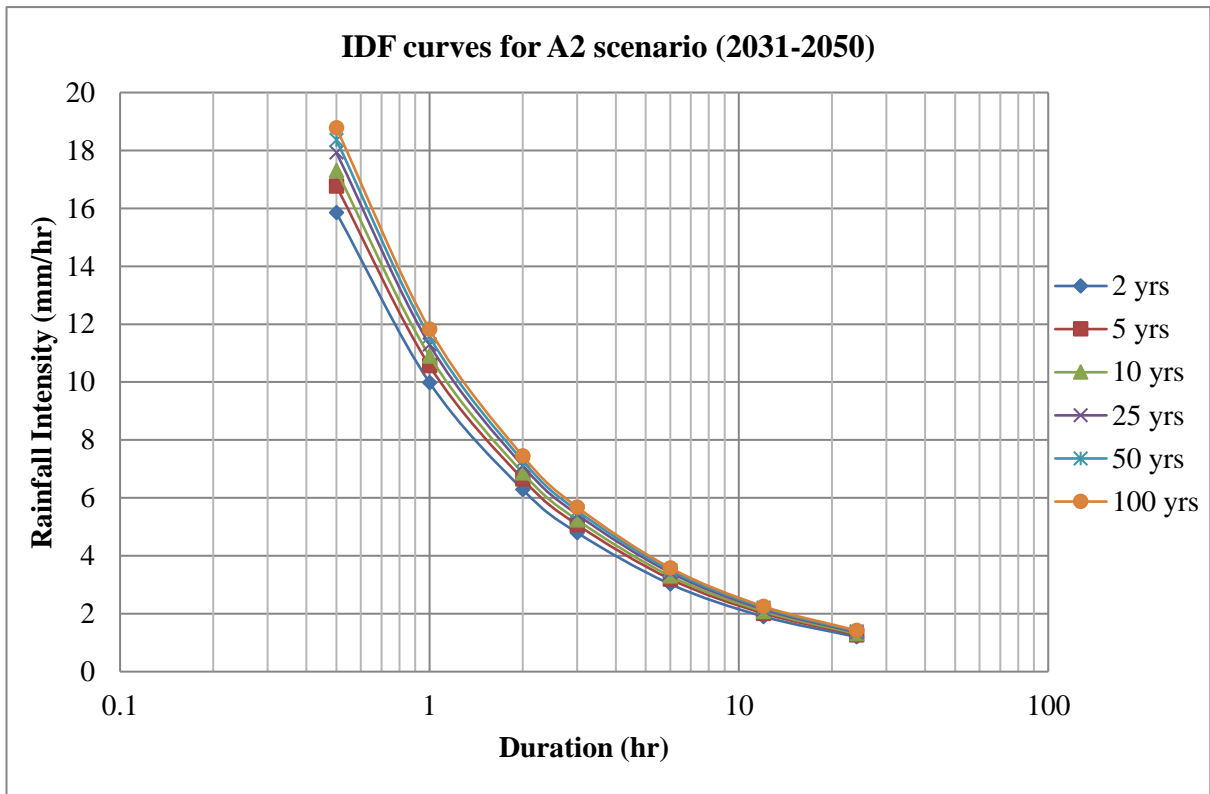


**Figure 5.5** IDF curve for A2 scenario (2031-2050)

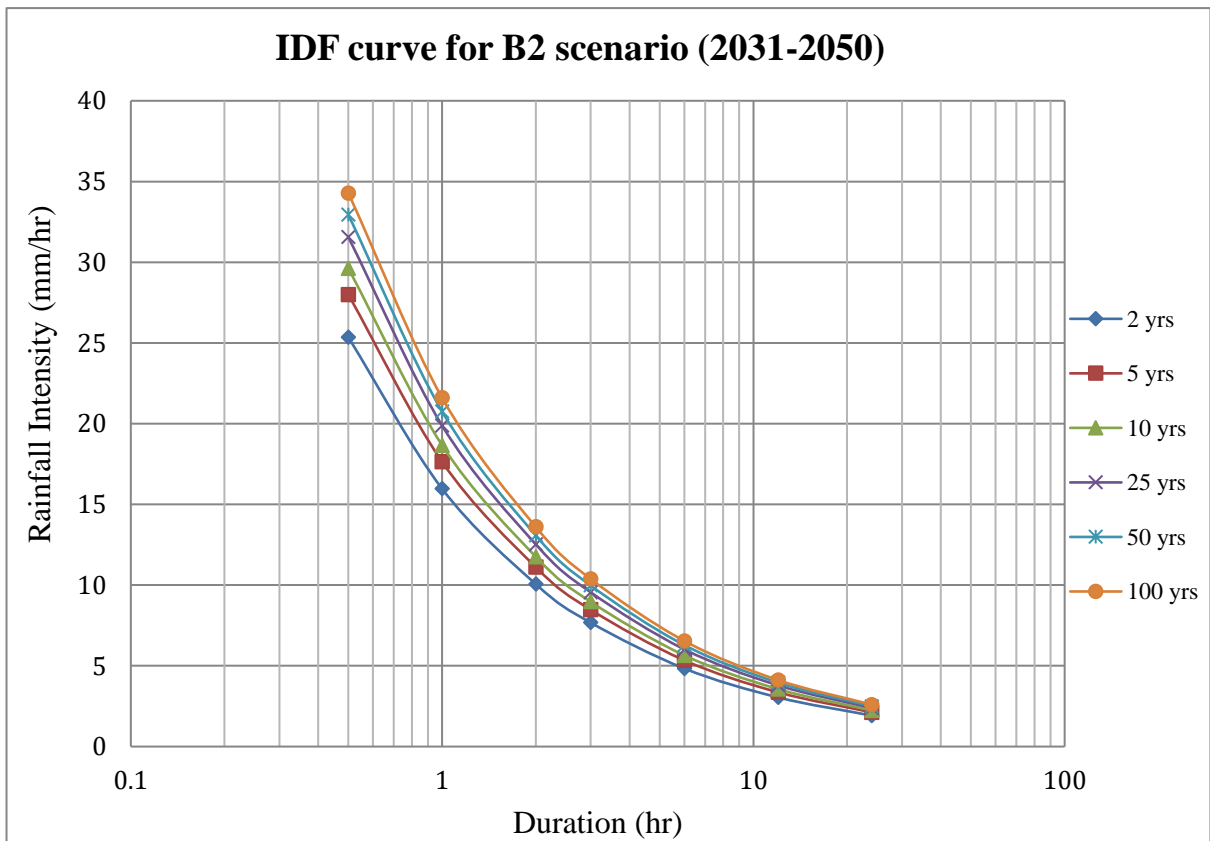


**Figure 5.6** IDF curve for B2 scenario (2031-2050)

#### 5.4.6 MATHEMATICAL EXPRESSIONS OF THE IDF CURVES

Instead of interpreting rainfall intensity from maps or graphs, the IDF connection may be stated using empirical equations. Therefore, a generic form is provided in Table 5.17, and for the stations that were taken into consideration, a mathematical expression was created to calculate severe rainfall intensities that exceeded the reported data. This expression makes use of the predicted IDF parameters for a particular duration and frequency.

**Table 5.16** IDF relationships under different climate scenarios

<b>Climate Scenerios</b>	<b>Year</b>	<b>IDF relationship</b>
Current climate	1979-2013	$I = \frac{39.02T_r^{0.21}}{T_d^{0.67}}$
A2 scenario	2011-2030	$I = \frac{9.86T_r^{0.05}}{T_d^{0.67}}$
	2031-2050	$I = \frac{9.81T_r^{0.04}}{T_d^{0.67}}$
B2 scenario	2011-2030	$I = \frac{15.38T_r^{0.08}}{T_d^{0.66}}$
	2031-2050	$I = \frac{15.45T_r^{0.07}}{T_d^{0.67}}$

## 5.5 GENERATION OF ISOPLUVIAL MAPS

The twenty-three rain gauge stations' rainfall data was used in ArcGIS using the Inverse Distance Weighted (IDW) algorithm for this purpose. For the ungauged Sites, the rainfall intensity estimate was extrapolated from other stations within the river basin. Isopluvial maps for a certain duration and return periods throughout the whole basin are developed using these data. The isopluvial maps for various 100-year return periods are shown in Figure 5.7.

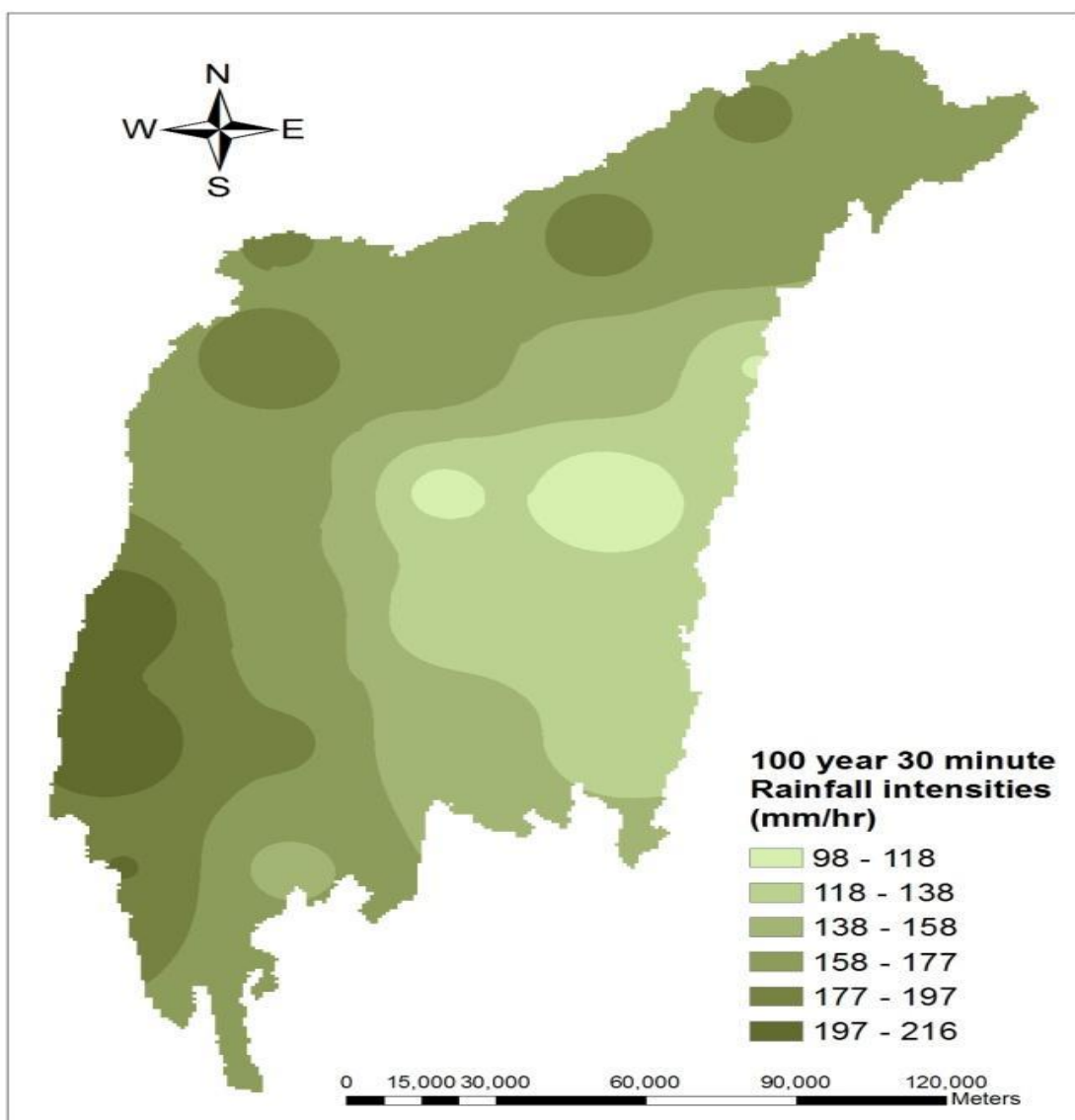


**Figure 5.7** Isopluvial maps for 30 minutes of 100-year return period for current climate.

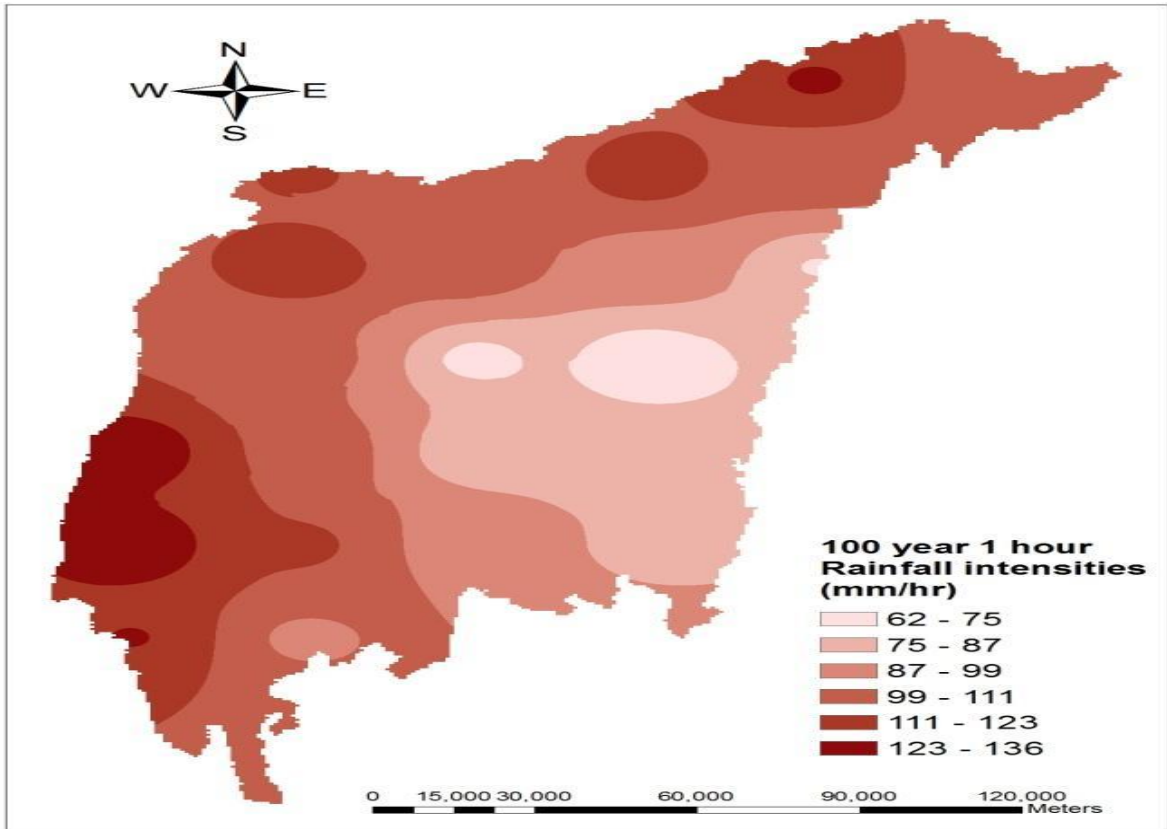


**Figure 5.8** Isopluvial maps for 1 hour of 100-year return period for current climate.

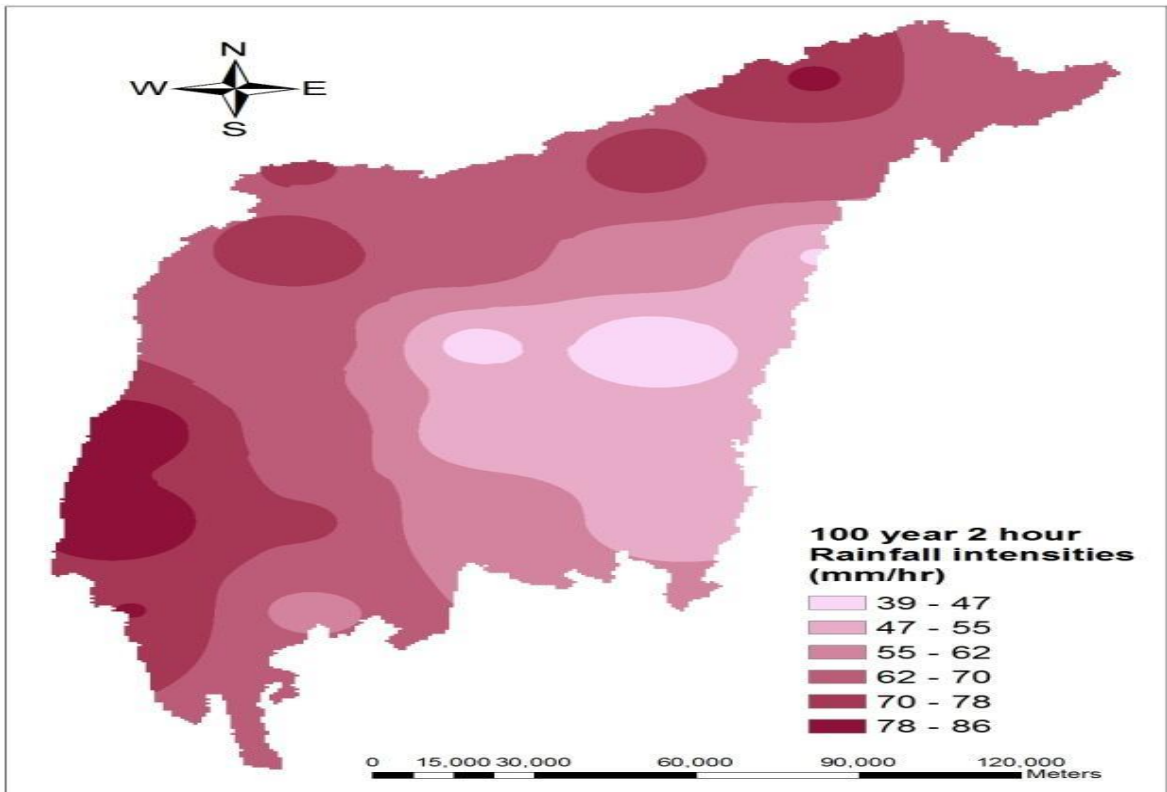


**Figure 5.9** Isopluvial maps for 2 hours of 100-year return period for current climate.

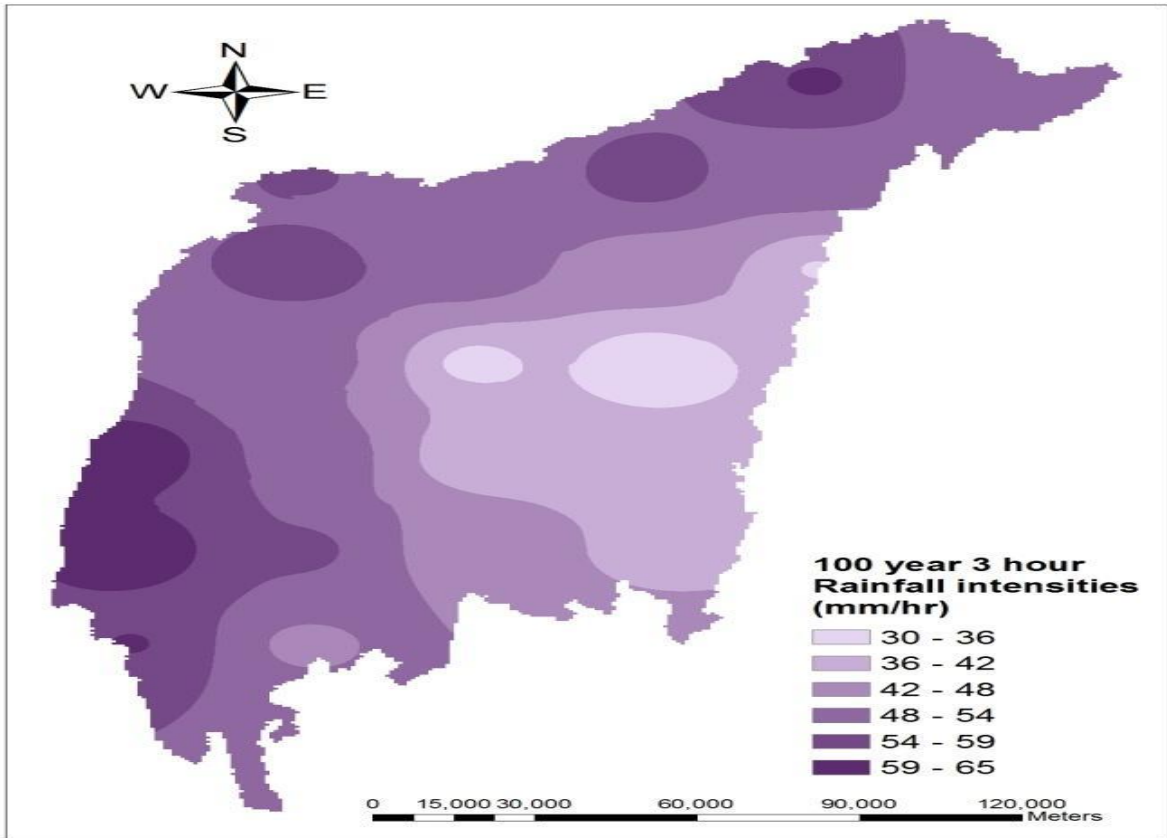


**Figure 5.10** Isopluvial maps for 3 hours of 100-year return period for current climate.

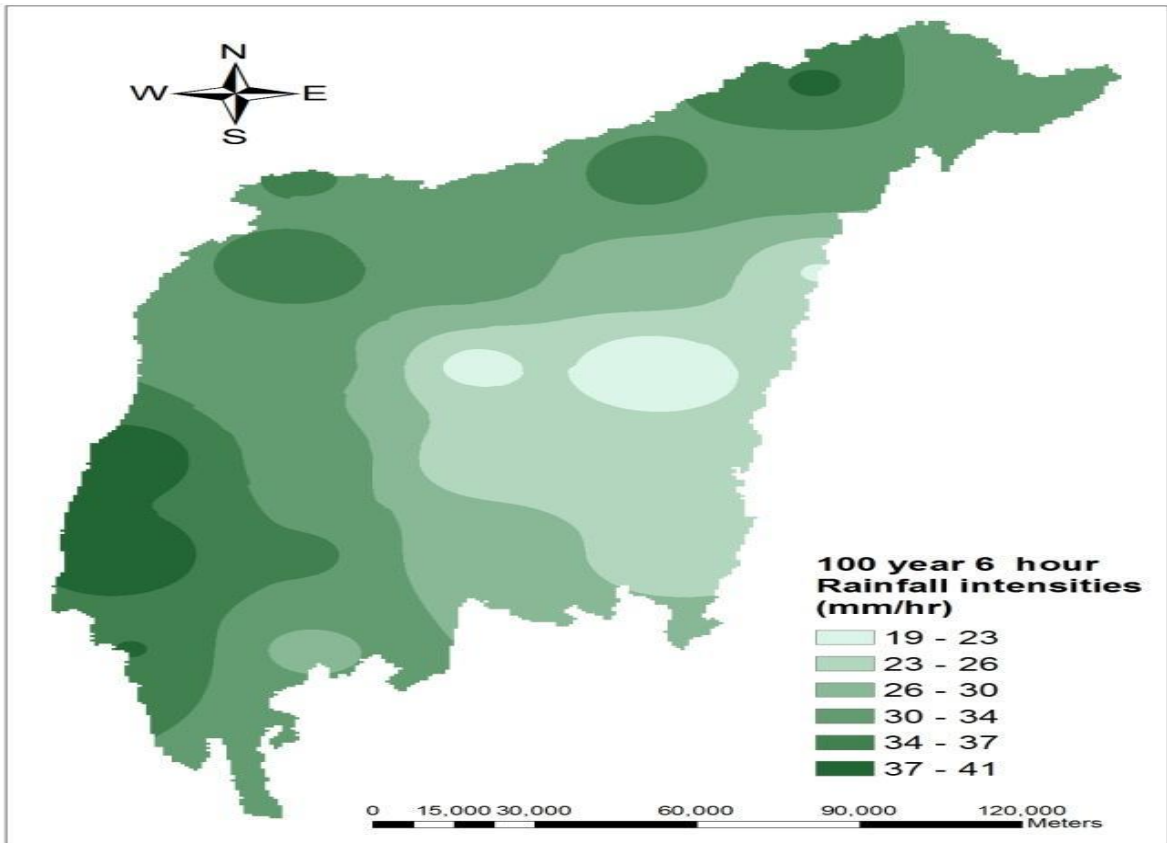


**Figure 5.11** Isopluvial maps for 6 hours of 100-year return period for current climate.

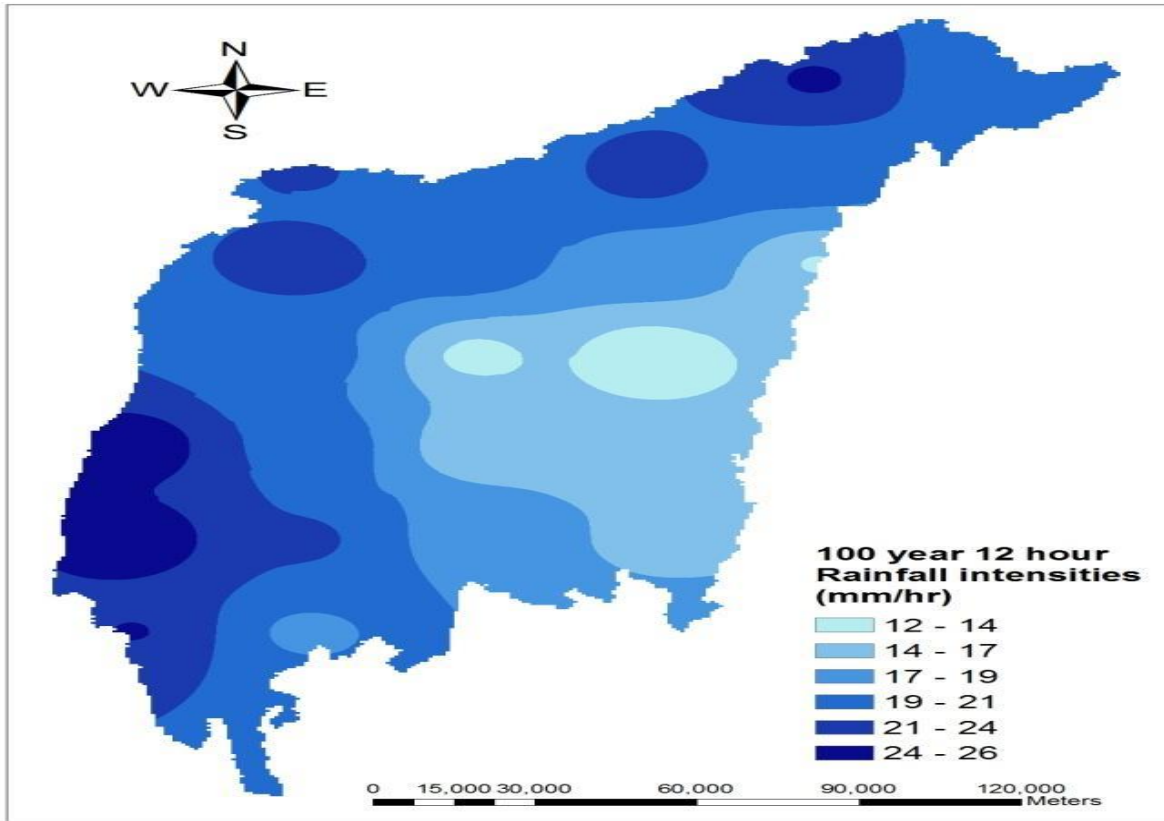


**Figure 5.12** Isopluvial maps for 12 hours of 100-year return period for current climate.

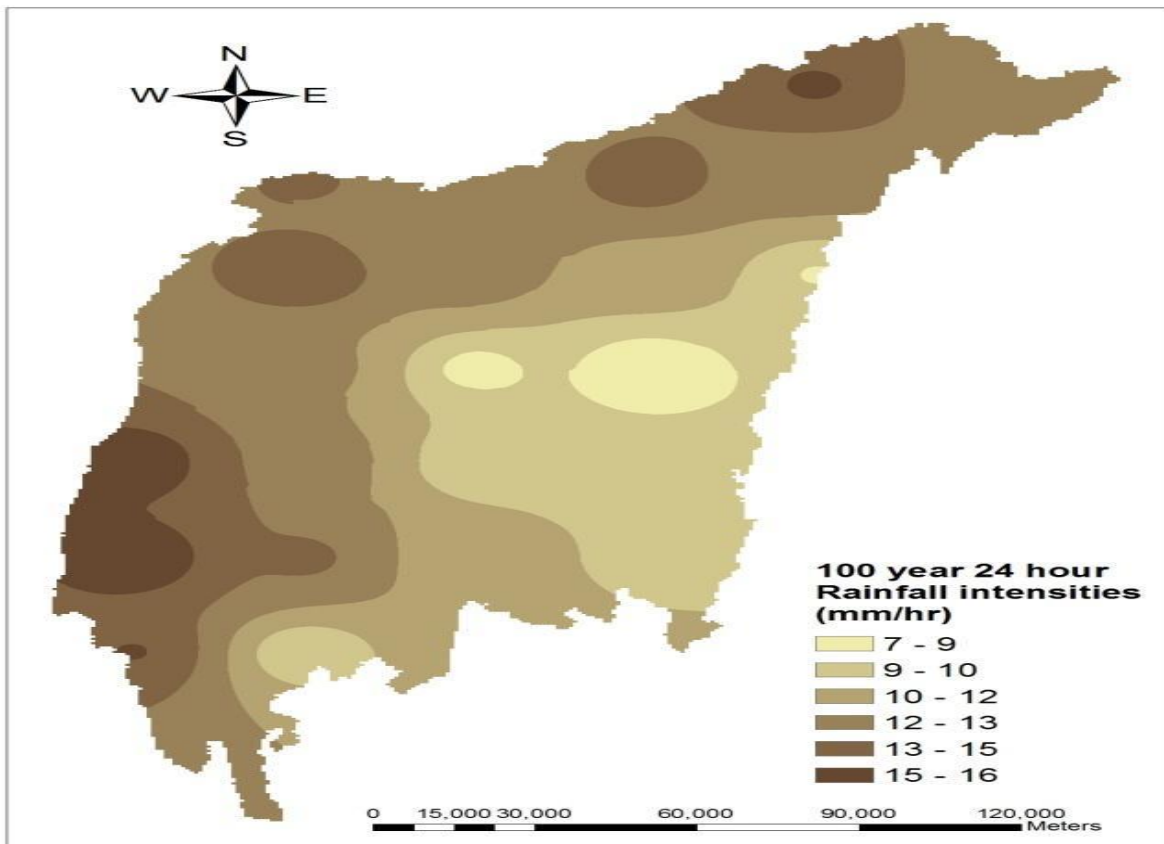


**Figure 5.13** Isopluvial maps for 24 hours of 100-year return period for current climate.

## 5.6 COMPARISON OF THE IDF RESULTS

For the purpose of quantifying the change in severe rainfall quantiles, the IDF findings were compared using IDF curves created under the developing climate change scenarios and the historic IDF connections for the stations that were taken into consideration. The relative difference between the curves was used to indicate the change in the rainfall intensity, which was obtained using (3.15). From Table 5.18 to Table 5.21, we can see the results of the relative difference that was produced.

**Table 5.17** Relative difference (RD) in intensity of rainfall from the current climate for A2 scenario (2011-2030) for different return periods

Duration (hr)	Relative Difference for A2 (2011-2030)					
	2	5	10	25	50	100
0.5	-123.7	-136.2	-142.5	-148.8	-152.8	-156.1
1	-123.7	-136.2	-142.5	-148.9	-152.9	-156.3
2	-123.7	-136.2	-142.5	-148.9	-153.5	-156.3
3	-123.6	-136.2	-142.5	-148.9	-153.4	-156.3
6	-123.7	-136.3	-142.5	-148.8	-154.0	-156.2
12	-123.8	-136.2	-142.7	-148.9	-153.0	-156.4
24	-123.8	-135.7	-142.0	-148.4	-152.5	-155.9

**Table 5.18** Relative difference (RD) in intensity of rainfall from the current climate for B2 scenario (2011-2030) for different return periods

Duration (hr)	Relative Difference for B2 (2011-2030)					
	2	5	10	25	50	100
0.5	-91.2	-104.7	-111.9	-119.6	-124.7	-129.0
1	-92.1	-104.3	-110.8	-118.1	-122.8	-127.0
2	-92.1	-104.3	-110.8	-118.0	-123.8	-127.0
3	-92.1	-104.3	-110.8	-118.0	-123.7	-127.0
6	-92.1	-104.3	-110.8	-118.1	-124.4	-127.1
12	-92.2	-104.3	-110.9	-118.1	-123.0	-127.1
24	-92.0	-103.2	-109.8	-117.2	-121.9	-126.2

**Table 5.19** Relative difference (RD) in intensity of rainfall from the current climate for A2 scenario (2031-2050) for different return periods

Duration (hr)	Relative Difference for A2 (2031-2050)					
	2	5	10	25	50	100
0.5	-124.3	-137.3	-143.7	-150.3	-154.3	-157.7
1	-124.2	-137.2	-143.7	-150.3	-154.4	-157.9
2	-124.2	-137.2	-143.7	-150.3	-155.1	-157.9
3	-124.2	-137.3	-143.8	-150.4	-155.0	-157.9
6	-124.3	-137.3	-143.8	-150.4	-155.5	-157.9
12	-124.1	-137.2	-143.8	-150.3	-154.4	-157.9
24	-124.3	-136.5	-143.1	-149.7	-153.9	-157.5

**Table 5.20** Relative difference (RD) in intensity of rainfall from the current climate for B2 scenario (2031-2050) for different return periods

Duration (hr)	Relative Difference for B2 (2031-2050)					
	2	5	10	25	50	100
0.5	-91.2	-105.3	-112.4	-120.0	-124.8	-129.0
1	-91.2	-105.2	-112.5	-120.2	-125.0	-129.3
2	-91.2	-105.2	-112.5	-120.1	-126.0	-129.3
3	-91.1	-105.2	-112.5	-120.2	-125.9	-129.3
6	-91.1	-105.2	-112.5	-120.2	-126.6	-129.3
12	-91.2	-105.4	-112.6	-120.3	-125.1	-129.3
24	-91.2	-104.2	-111.6	-119.3	-124.4	-128.5

# CHAPTER 6

## CONCLUSION

---

---

### 6.1 CONCLUSION

This study is an indication of studies on IDF curves generated for the Barak River Basin under changing climate circumstances.

We used daily rainfall data acquired from Global Weather Data for SWAT in the HadCM3 model, and for the same area, we included SDSM predictors retrieved from the CCISC data portal. Directly downloading all of the data files was the next stage in establishing SDSM. In this case, we used SDSM to downscale the rainfall for the research area. This method takes climate data from global warming modellers' coarse resolution and brings it down to the level of individual sites or locations. When the scenarios were being created, HadCM3A2 and HadCM3B2 were the two output files used for emissions. Preliminary analysis was conducted to guarantee the consistency of the data gathered. The disaggregation of daily rainfall was accomplished using the IMD one-third reduction technique.

By calculating the coefficient of determination ( $R^2$ ), the best distribution for the probabilities was selected. To make sure the probability distribution was well-fitted, we used the EasyFit application to run the Anderson-Darling, Chi-Squared, and Kolmogorov-Smirnov tests. By determining the size of the Thiessen polygon for each station using ArcGIS, the average Intensity-Duration-Frequency curve for the study region was created. By simulating the impact of climate change on the IDF curves using SDSM, the base period and future climate change scenarios was constructed. We made Intensity-Duration-Frequency (IDF) curves for predicted rainfall and compared them with the future scenarios. For each possible future climate, we estimated the relevant IDF parameters, established IDF connections, and produced isopluvial maps. For each of the 23 sites and the return periods, we estimated the IDF parameters and derived the mathematical equations for the IDF curves as a function of climatic change.

- For the A2 scenarios from the year 2011-2030 and 2031-2050 the IDF curve in the figure 5.3 and figure 5.5 respectively shows a gradual decrease in the rainfall intensity as for the 100 years return periods, we have a decrease of rainfall intensity from (19.58-18.78) mm for the duration of 0.5hr and (1.48-1.42) mm for the duration of 24hr.
- For the B2 scenarios from the year 2011-2030 and 2031-2050 the IDF curve in the figure 5.4 and figure 5.6 respectively shows a gradual decrease in the rainfall intensity as for the 100 years return periods, we have a decrease of rainfall intensity from (34.35-34.27) mm for the duration of 0.5hr and (2.7-2.59) mm for the duration of 24hr.

Looking at the historical IDF curves Fig 5.2 compared to the IDF curve under both climate change scenarios (A2 and B2) Fig 5.3, Fig 5.4, Fig 5.5, Fig 5.6 shows a significant decrease in the number of rainfall intensities for the future climate.

## **6.2 SCOPE FOR FURTHER STUDY**

In this study one downscaling method and one general circulation model (GCM) is used. In future, more research is needed to include various scenarios, GCMs, and downscaling techniques in order to account for the potential impacts of climate change. Considering the significant level of uncertainty in GCM results, future research may also investigate doing detailed analysis.

## REFERENCES

- 1) Akbari, H., Rakhshanderoo, G. R., Afrooz, A., and Pourtouserkani, A. (2015). "Climate Change Impact on Intensity-Duration-Frequency Curves in Chenar-Rahdar River Basin, Southern Iran." *EWR/ Watershed Management Symposium*, ASCE Headquarter, Reston, VA, USA, 48-61.
- 2) Al-anazi, K. K., and El-Sebaie, I. H. (2013). "Development of Intensity-Duration-Frequency Relationships for Abha City in Saudi Arabia." *International Journal of Computational Engineering Research*, 3(10), 58-65.
- 3) Alemaw, B. F., and Chaoka, R. T. (2016). "Regionalization of Rainfall Intensity-Duration-Frequency (IDF) Curves in Botswana." *Journal of Water Resource and Protection*, 8, 1128-1144.
- 4) Al-Hussoun, S. A. (2011). "Developing an empirical formula to estimate rainfall intensity in Riyadh region." *Journal of King Saud University- Engineering Sciences*, 23(2), 81-88.
- 5) Al-Shaikh, A. A. (1985). "Rainfall frequency studies for Saudi Arabia", thesis, presented to King Saud University, Riyadh (K.S.A) in partial fulfilment of the requirements for the degree of Master of Science.
- 6) Bora, K., and Choudhury, P., (2015). "Estimation of Annual Maximum Daily Rainfall of Silchar, Assam." *International Conference on Engineering Trends and Science and Humanities*, Imayan College of Engineering, Tamil Nadu, India, 12-16.
- 7) Carlier, E., and Khattabi, J. E. (2016). "Impact of Global Warming on Intensity-Duration-Frequency (IDF) Relationship of Precipitation: A Case Study of Toronto, Canada." *Open Journal of Modern Hydrology*, 6(1), 1-7.
- 8) Chow, V. T., Maidment, D. R., and Mays, L.W. (1988). *Applied Hydrology*, 2<sup>nd</sup> Ed., McGraw-Hill, New York.
- 9) Coulibaly, P., and Shi, X. (2005). "Identification of the Effect of Climate Change on Future Design Standards of Drainage Infrastructure in Ontario." Report, Ministry of Transportation of Ontario, Canada.
- 10) Dar, A. Q., and Maqbool, H. (2016). "Rainfall Intensity-Duration-Frequency Relationship for different regions of Kashmir Valley (J&K) India." *International Journal of Advance Research in Science and Engineering*, 5(1), 113-125.
- 11) Das, R., Goswami, D., and Sharma, B. (2016). "Generation of Intensity Duration Frequency Curve using Short Duration Rainfall Data for Different Return Period for Guwahati City." *International Journal of Scientific and Engineering Research*, 7(7), 908-911.

- 12) Deka, R. L., Mahanta, C., Pathak, H., Nath, K. K., and Das, S. (2012). "Trends and fluctuations of rainfall regime in the Brahmaputra and Barak Basins of Assam, India." *Theoretical and Applied Climatology*, 14(1), 61-71.
- 13) Elsebaie, I. H. (2012). "Developing Rainfall Intensity-Duration-Frequency Relationship for Two Regions in Saudi Arabia." *Journal of King Saud University- Engineering Sciences*, 24(2), 131-140.
- 14) Ewea, H. A., Elfeki, A. M., and Al-Amri, N. S. (2016). "Development of Intensity-Duration- Frequency Curves for the Kingdom of Saudi Arabia." *Geomatics, Natural Hazards and Risk*, 1-15.
- 15) Gebreslassie, B. (2014). "Spatial and Temporal Rainfall Intensity-Duration-Frequency Parameters Variability for Awash River Basin, Ethiopia." thesis, presented to Haramaya University, Ethiopia in partial fulfilment of the requirements for the degree of Master of Science.
- 16) Hosking, J. R. M., and Wallis, J. R. (1993). "Some Statistics Useful in Regional Frequency Analysis." *Water Resources Research*, 29(2), 271-281.
- 17) IPCC, (2007a). "Climate Change 2007: The Physical Science Basis. Contribution of Working Group I to the Fourth Assessment Report of the Intergovernmental Panel on Climate Change." [Solomon, S., D. Qin, M. Manning, Z. Chen, M. Marquis, K.B. Averyt, M. Tignor and H.L. Miller (editors.)]. Cambridge University Press, Cambridge, United Kingdom and New York, USA.
- 18) Kuok, K. K., Mah, Y. S., Imteaz, M. A., and Kueh, S. M. (2016). "Comparison of Future Intensity Duration Frequency Curve by considering the Impact Of Climate Change: Case Study For Kuching City." *International Journal of River Basin Management*, 14 (1), 47-55.
- 19) Mirhosseini, G., Srivastava, P., and Stefanova, L. (2012). "The Impact of Climate Change on Rainfall Intensity-Duration-Frequency (IDF) Curves in Alabama." *Regional Environmental Change*, 13(1), 25-33.
- 20) Peck, A., Prodanovic, P., and Simonovic, S. P. (2012). "Rainfall Intensity Duration Frequency Curves under Climate Change: City of London, Ontario, Canada." *Canadian Water Resources Journal*, 37(3), 177-189.
- 21) Prodanovic, P., and Simonovic, S. P. (2007). "Development of Rainfall Intensity Duration Frequency curves for the City of London under the Changing Climate". *Water Resources Research*.
- 22) *Report no. 058*, Facility for Intelligent Decision Support, Department of Civil and Environmental Engineering. London, Ontario, Canada.

- 23) Rashid, M. M., Faruque, S. B., and Alam, J. B. (2012). "Modelling of Short Duration Rainfall Intensity Duration Frequency (SDR-IDF) Equation for Slyhet City in Bangladesh." *ARPN Journal of Science and Technology*, 2(2), 92-95.
- 24) Rasel, M., and Islam, M. (2015). "Generation of Rainfall-Duration-Frequency Relationship for North-Western Region in Bangladesh." *IOSR Journal of Environmental Science, Toxicology and Food Technology*, 9(1), 41-47.
- 25) Reddi, P.J. (2002). *A Text Book of Hydrology*. Laxmi Publications Pvt. Ltd., New Delhi.
- 26) Sarkar, S., Goel, K., and Mathur, B. S. (2010). "Development of Isopluvial Map using L-moment Approach for Tehri-Garhwal Himalaya." *Stochastic Environmental Research and Risk Assessment*, 24(3), 411–423.
- 27) Sharma, R., Choudhury, N., Alam, R., Seleyi, V., and Sangtam, Y. (2016). "Development of Intensity-Duration-Frequency Curves for precipitation in Western Watershed of Guwahati (Assam)." *International Journal of Latest Trends in Engineering and Technology*, 6(4), 575-579.
- 28) Sharma, P. J., Patel, P. L., and Jothiprakash, V. (2016). "At-Site Flood Frequency Analysis for Upper Tapi Basin, India." 21st International Conference on Hydraulics, Water Resources and Coastal Engineering (HYDRO 2016), CWPRS, Pune, 1-10.
- 29) Singh, R., Arya, D. S., Taxak, A. K., and Vojinovic, Z. (2016). "Potential Impact of Climate Change on Rainfall Intensity-Duration-Frequency Curves in Roorkee, India." *Water Resources Management*, 30(13), 4603-4616.
- 30) Souvignet, M., Gaese, H., Ribbe, L., Kretschmer, N., and Oyarzun, R. (2010). "Statistical Downscaling of Precipitation and Temperature in North-Central Chile: An Assessment of Possible Climate Change Impacts in an Arid Andean Watershed." *Hydrological Sciences Journal*, 55(1), 41-57.
- 31) Subyani, A. M., and Al-Amri, N. S. (2015). "IDF and Daily Rainfall Generation for Al-Madinah city, Western Saudi Arabia." *Arabian Journal of Geosciences*, 8(12), 11107-11119.
- 32) Wagesho, N., and Claire, M. (2016). "Analysis of Rainfall Intensity-Duration-Frequency Relationship for Rwanda." *Journal of Water Resource and Protection*, 8(7), 706-723.
- 33) Wilby, R. L., and Dawson, C. W. (2007). "SDSM 4.2- A decision support tool for the assessment of regional climate change impacts".
- 34) Zope, P. E., Eldho, T. I., and Jothiprakash, V. (2016) "Development of Rainfall Intensity Duration Frequency Curves for Mumbai City, India." *Journal of Water Resource and Protection*, 8, 756-765.